UNIVERSITY OF OKLAHOMA

GRADUATE COLLEGE

STRATIGRAPHIC VARIABILITY OF MISSISSIPPIAN MERAMEC CHEMOFACIES AND PETROPHYSICAL PROPERTIES USING MACHINE LEARNING AND GEOSTATISTICAL MODELING, STACK TREND, ANADARKO BASIN, OKLAHOMA

A THESIS

SUBMITTED TO THE GRADUATE FACULTY

in partial fulfillment of the requirements for the

Degree of

MASTER OF SCIENCE

By

LURA HARDISTY

Norman, Oklahoma

2019

STRATIGRAPHIC VARIABILITY OF MISSISSIPPIAN MERAMEC CHEMOFACIES AND PETROPHYSICAL PROPERTIES USING MACHINE LEARNING AND GEOSTATISTICAL MODELING, STACK TREND, ANADARKO BASIN, OKLAHOMA

A THESIS APPROVED FOR THE

SCHOOL OF GEOSCIENCES

BY THE COMMITTEE CONSISTING OF

Dr. Matthew Pranter, Chair

Dr. Kurt Marfurt

Dr. Deepak Devegowda

ACKNOWLEDGEMENTS

This research was made possible through the funding provided by the Reservoir Characterization and Modeling Laboratory and Marathon Oil Corporation. I would like to recognize Marathon Oil Corporation, Oklahoma Petroleum Information Center (OPIC) and the Integrated Core Characterization Center for providing data. I thank Dr. Carl Sondergeld, Dr. Chandra Rai, Dr. Deepak Devegowda and Dr. Kurt Marfurt for their guidance, feedback and support through the duration of this project. I thank Dr. Ali Tinni, Connor Holasek, Dick Larese, Heyleem Han, Ishank Gupta, and Son Dang for numerous data and machine learning guidance that have been integrated into this research. I would like to recognize the software providers Schlumberger, The Easycopy Company and R for Petrel, EasyCore and R Studio which allowed me to conduct this study. I would like to acknowledge Micaela Langevin for all of her support and communications between Marathon Oil Corporation, the Reservoir Characterization and Modeling Lab and the Integrated Core Characterization Center.

I thank Dr. Pranter for his advice, input, guidance and mentorship throughout this research and the Master's degree as a whole. I would like to thank the RCML group, both past and present, for their support, insight and friendship. I would like to thank Thorn McMartin for all of his support and love that got me through these challenging years of personal and academic growth. I thank my parents and family for their love and support. Lastly, I would like to thank God for blessing me with the opportunity to work with and be mentored by such a remarkable group of people, and the lessons I've learned throughout the duration of my Master's degree.

TABLE OF CONTENTS

ABSTRACT

Mississippian deposits and reservoirs in the STACK play (Sooner Trend in the Anadarko [Basin] in Canadian and Kingfisher counties) of central Oklahoma are comprised of silty limestones, calcareous siltstones, argillaceous-calcareous siltstones, argillaceous siltstones and mudstones. Using core-derived X-ray fluorescence (XRF) data and established environmental proxies, the occurrence of specific elements is evaluated and their stratigraphic variability is illustrated. Other proxies are developed for indicator elements based on correlation to established proxies as well as background knowledge on how elements are associated with different minerals, rocks, and organic matter. For the Meramec, six indicator elements or element ratios serve as proxies for clay, detrital sediment, carbonate deposits and calcite cement, and biogenic and continentally derived quartz. Detailed core descriptions and an unsupervised K-means classification were used to cluster elemental data to develop three chemofacies: 1) calcareous sandstone, 2) argillaceous-calcareous siltstone and 3) detrital mudstone. Using a Random Forest approach, core-derived chemofacies were related to well logs and classified in non-cored wells to create chemofacies logs with an overall accuracy of 83%.

Core-derived XRF, well logs, and chemofacies logs were integrated to produce a dip-oriented cross-sectional chemofacies model that trends from the northwest to southeast across the southern STACK trend. Chemofacies distributions exhibit the transgressive-regressive-transgressive cycles of the Meramec. The Meramec is composed of seven stratigraphic zones. The stratigraphic variability of chemofacies shows an increase of argillaceous detrital mudstone from the Meramec 1, 2 to the Meramec 3 which is capped by a maximum flooding surface. From the Meramec 4 to the Meramec 5, an increase of the argillaceous-calcareous siltstone and calcareous sandstone represents a progradational shoreline. Rock types, porosity, water

saturation and reservoir quality were also modeled to determine the petrophysical properties distributions and how certain petrophysical properties are associated with each chemofacies. A porosity model exhibits an increase in porosity from the calcareous sandstone to detrital mudstone. The average water saturations per chemofacies indicates high water saturation associated with the argillaceous-calcareous siltstone, moderate water saturation associated with calcareous sandstone and low water saturation associated with detrital mudstone. Ideal reservoir quality of chemofacies based on petrophysical properties indicates high reservoir quality within the detrital mudstone and low reservoir qualities in both the argillaceous-calcareous siltstone and calcareous sandstone. Biogenic quartz is associated with drilling issues, specifically frequent bit trips due to its hardness. Interpreted biogenic quartz from element profiles correspond to the calcareous sandstone chemofacies which can be predicted from triple combo logs and mapped. Petrophysical property distributions reflect the stratigraphic variability of chemofacies and rock types throughout the models.

INTRODUCTION

The Mississippian Meramec in the eastern Anadarko basin of central Oklahoma consists of a succession of upward coarsening cycles of argillaceous to calcareous fine-grained sandstones, siltstones and mudstones that form major petroleum reservoirs. In central Oklahoma, Mississippian strata is characterized by a mixed siliciclastic and carbonate system that consists of mixed siliceous and calcareous sandstones, siltstones and mudstones (Price et al., 2017; Drummond, 2018; Duarte, 2018; Hardwick, 2018; Hickman, 2018; Leavitt, 2018; J. Miller, 2018; M. Miller, 2019; Terrell, 2019). Many studies have focused on the deposition and reservoir properties of the Mississippian in northern Oklahoma and southern Kansas (Figure 1). To the north, Mississippian strata is composed of a chert-rich carbonate with the dominate reservoir being a porous tripolitic chert (Peeler 1985; Parham and Northcutt, 1993; Watney et al., 2001; Mazzullo, 2011; Grammer et al., 2013; LeBlanc, 2014; Flinton, 2016; Mazzullo et al., 2016; Lindzey et al., 2017; Turnini et al., 2017; Wethington, 2017; Price and Grammer, 2018; Drummond, 2018). Flinton (2016) studied the sequence stratigraphy of the Mississippian limestone using cores and well logs to identify six depositional lithofacies. Flinton (2016) observed vertical stacking patterns within these lithofacies that were indicative of four periods of sea level cyclicity. He interpreted the Mississippian strata to be a 2^{nd} order supersequence nested with four 3^{rd} order sequences, each of which contains 4^{th} order and 5^{th} order sequences driven by Milankovitch cyclicity. Flinton concluded that the cyclicity of the eustatic and relative sea level, as represented by the Mississippian limestone by the 2^{nd} order supersequence and associated subsequences, controlled the creation and distribution of the hydrocarbon reservoirs. Studying the spatial lithology and distribution of the highly porous tripolitic chert within Mississippian strata in northern Oklahoma, Lindzey (2015) observed that vertical production was influenced by

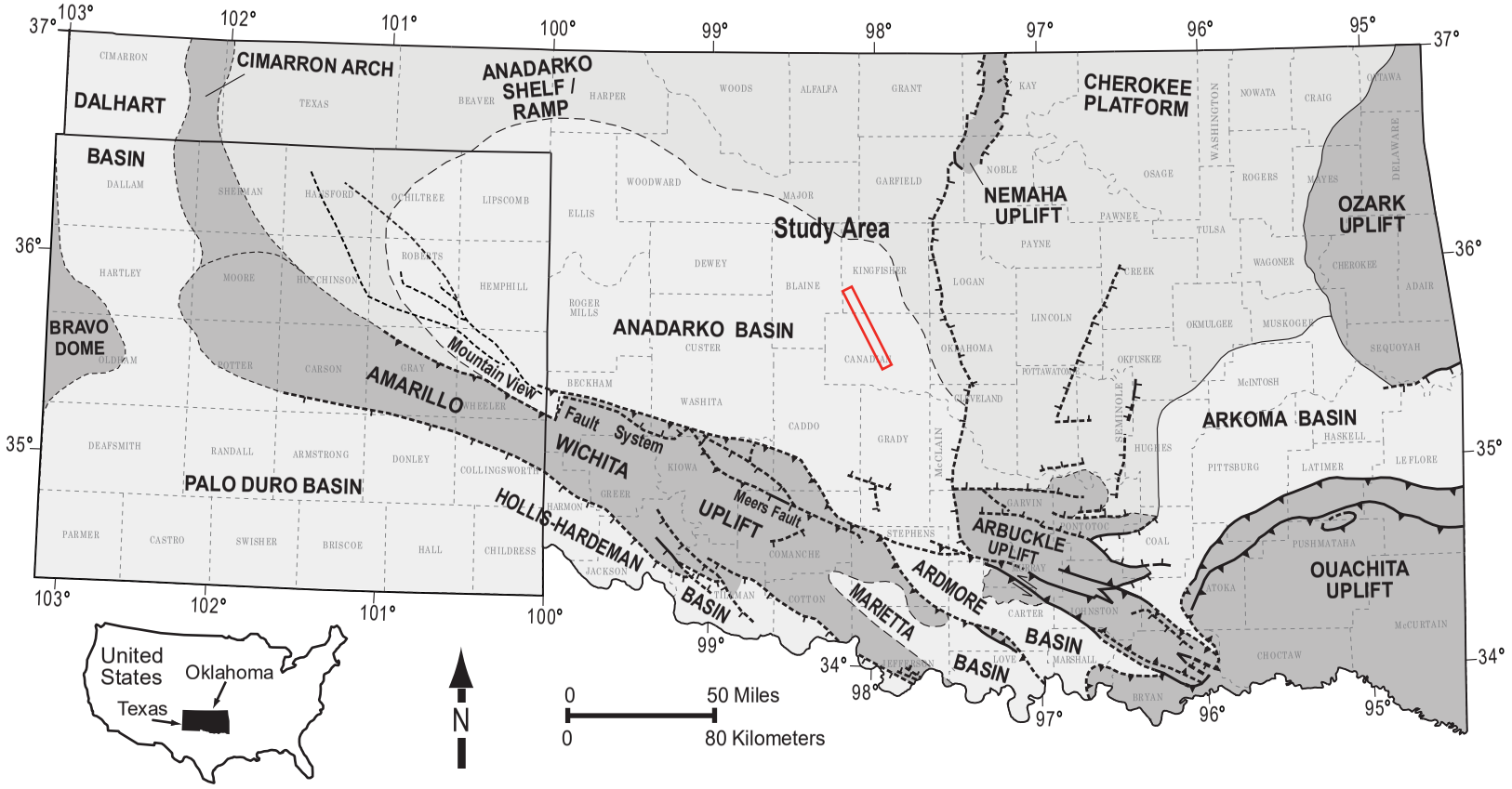

Figure 1: Regional map of major tectonic provinces of Oklahoma and part of Texas. Modified from Dutton, 1985; Campbell et al., 1988; McConnell et al., 1989; Northcutt and Campbell, 1995; Johnson and Luza, 2008; LoCricchio, 2012.

tripolite, whereas horizontal production was most influenced by water saturation and the porosity of chert-rich limestone. Further work on tripolitic chert in northern Oklahoma was done by Turnini (2015) who observed seven key lithologies of the Mississippian aged strata, tripolitic chert being the primary reservoir lithology of the Mississippian. Turnini concluded that although there was a direct relationship between fluid production and the tripolitic chert thickness, there was not a direct relationship between the lithology's thickness and oil production. Within the primary study area, to the south of this thoroughly studied Mississippian limestone, less work has been done. Leavitt (2017) determined sedimentation of the Meramecian silts to be derived from aeolian processes. Price et al. (2017) studied lithologic controls on reservoir quality. Price concluded calcite cement to be the primary driver of reservoir quality, attributing the preservation of primary porosity to be a key role of clay within the Meramec. Hardwick (2018) found that calcite-cement in Meramecian siltstones significantly obstructed porosity and can act as seals to flow, while clay-filled matrices provided preservation of primary porosity. Drummond (2018), Hickman (2018), Miller (2018) and Miller (2019) identified lithofacies from cores within the Meramec that were composed of a mixed siliceous-calcareous siltstones and heavily bioturbated and laminated mudstones with stacking patterns that indicate shallowing upward cycles capped by flooding surfaces. Drummond (2018) and Miller (2019) found that basinward, lithofacies become dominated by calcite-cemented argillaceous and siliceous lithologies rather than the carbonate limestones observed in the northwest.

To expand upon previous work, this study addresses the stratigraphy and environmental conditions of the Meramec Series and to further clarify how chemical composition and depositional facies may vary spatially. To accomplish those goals, this study addresses the following research questions:

1) What are the elemental distributions that define chemofacies and how do they relate to environmental conditions?
2) What is the chemostratigraphic framework and spatial distribution of chemofacies within that framework?
3) How does the distribution of chemofacies compare to rock types and petrophysical property distributions?
4) How do chemofacies, rock types and petrophysical properties relate to production?

To address the research questions, this study defines chemofacies in cored wells, classifies chemofacies in noncored wells, and models chemofacies along a proximal to distal, dip-oriented cross section to evaluate the stratigraphic variability of chemofacies. Data include core-derived x-ray fluorescence (XRF) from 5 cored wells, 5 wells with production data, XRF-derived mineralogy, 24 non-cored wells with triple-combo logs (gamma-ray, neutron porosity and bulk density, etc.) and 456 thin-section photomicrographs from 1 cored well. Chemofacies are defined by elements used as proxies for environmental conditions during deposition. These proxies are determined based on inter-elemental correlation between elements with established environmental proxies and confirmed by thin sections and core observations. These key elements are referred to as indicator elements and are clustered and interpreted to define chemofacies. Zonation of strata are determined based on chemofacies stacking patterns and chemostratigraphic profiles of detrital-sourced element proxies. Chemofacies are classified in non-cored wells through a machine learning technique called Random Forest. The spatial distribution of chemofacies is determined by generating a dip-oriented cross-sectional 3-D chemofacies model. Spatial variability of chemofacies, rock types and reservoir properties are evaluated and

compared to production data. The results illustrate relationships between well productivity and elementally derived facies, as well as petrophysical property distributions.

GEOLOGIC SETTING

The Anadarko Basin is an asymmetrical foreland basin (structurally deepest along the southern boundary) that trends to the northwest across Oklahoma, Texas Panhandle, southwestern Kansas, and southeastern Colorado (Beebe, 1959; Lane and De Keyser, 1980; Gutschick and Sandberg, 1983; Perry, 1989; Ball et al., 1991). The Anadarko Basin is bound by the Wichita uplift to the south, the Nemaha uplift to the east and the Anadarko shelf to the north (Campbell et al., 1988; Ball et al., 1991; Northcutt and Campbell, 1995). The Anadarko Basin is also bordered by the Cimarron arch that trends to the north from the Amarillo-Wichita uplift (Alder et al., 1987; Ball et al., 1991).

The results of the proto-Atlantic closure commenced during the Late Mississippian time. The collision between ancient continents, Paleozoic North America and Gondwana, brought about two orogenic events including the Ouachita and Wichita orogenies that lasted into the Permian. As the continents converged, the Wichita Mountains and Amarillo arch were uplifted and thrusted over the southern border of the southern Oklahoma aulacogen initiating the subsidence of the Anadarko Basin (Ball et al., 1991).

Mississippian strata in the midcontinent are made up of 4 major series including Kinderhook, Osage, Meramec and Chester (Figure 2). The Kinderhookian strata are the oldest of the Mississippian-aged rocks and reach a maximum thickness of 50 ft (15.24 m). In the Anadarko basin, the Osagean Series overlies the Kinderhookian strata and are thickest in the northwest and thin towards the southeast, the maximum thickness is 175 ft (53.34 m). Thin units

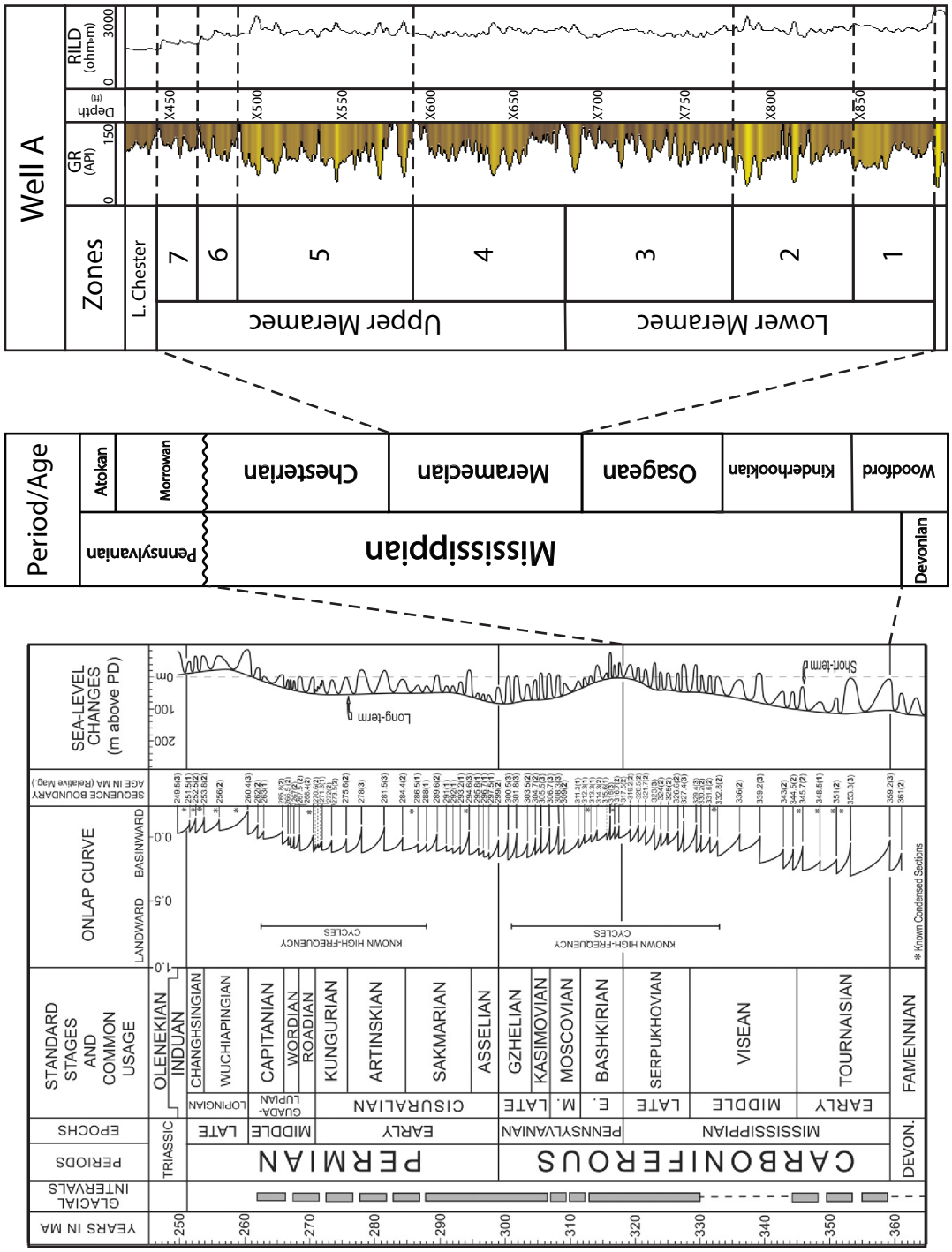

Figure 2: Mississippian stratigraphic column is displayed next to the sea level cyclicity of the Carboniferous and Permian periods. The Meramec is deposited during increasing cyclicity due in part to the climatic transition of the Mississippian, resulting in complex stacking patterns and lateral distribution of facies. (Modified from Boyd, 2008; Haq and Schutter, 2008; Miller, 2019)

of the Osage in the south are truncated and are overlain with angular unconformity by beds of the Meramec Series. The Meramecian strata thickens to the southeast and thins by truncation and onlap onto the paleo-uplifted regions which are now located at the margins of the Anadarko Basin. The Chesterian Series is the youngest of the Mississippian aged strata and thickens towards the north (Beebe, 1959; Curtis and Champlin, 1959; Alder et al., 1987; Northcutt et al., 2001).

Mississippian deposition in modern day central Oklahoma was located in a subtropical to tropical region at about 20° to 30° latitude south of the paleoequator (Curtis and Champlin, 1959). Meramec sediments were deposited during a climatic transition from greenhouse conditions to icehouse conditions on a gently sloping ramp. Early Mississippian deposits were a result of low amplitude sea-level fluctuations as a result of greenhouse conditions while icehouse conditions of the Late Mississippian consisted of higher amplitude sea-level changes (Read, 1995; Haq and Schutter, 2008). Climatic changes, Milankovich cycles, tectonics and sedimentation rates all play significant roles in the resulting high-frequency sea-level cyclicity, which contributes to the complex stacking patterns and lateral variability of facies (Comer, 1991; Haq and Schutter, 2008; Birch, 2015; Flinton, 2016; Price, 2017).

METHODS

Core Descriptions

Core descriptions are made to build background knowledge of lithologies, grain size, sedimentary structures, bioturbation, fractures, cements and fossils in the Meramec. Core descriptions for three cores (Appendix-B1) including Well A (475 ft; 144.8 m), Well B (516 ft; 157.3 m) and Well C (373 ft; 113.7 m) are used to develop interpretations of element

distributions within chemofacies. Thin sections from Well A are also used to determine cement from carbonate grains, quartz and clay content. The core descirptions and thin section analysis contribute to the understanding how the elements are materialized in lithologies and cements during the selection of indicator elements from the XRF data used to determine environmental conditions. Once chemofacies were determined, thin sections from depths of each chemofacies were analyzed to confirm element proxies and lithologies associated with chemofacies. Figure 3 shows the overall methodology.

Matrix Correlation

To determine the proper use of environmental proxies, the elements from XRF data are correlated within a matrix. Due to elements existing in multiple minerals and mineral assemblages, a linear relationship between elements is applied. A simple matrix correlation was created and interpreted based on the magnitude of each correlation coefficient. Strong correlations include coefficients greater than 0.75 or less than -0.75. Intermediate correlations are between 0.5 and 0.75 or -0.5 and -0.75. Correlations less than |0.5| are considered weak. Immobile elements with distinct origin are useful for relating to elements that can be associated with multiple minerals. For instance, titanium and zirconium are both highly immobile elements during diagenesis, but titanium can be incorporated into minerals associated with aeolian sedimentation. When titatium and zirconium have a low correlation coefficient, aeolian sedimentation can be interpreted. Another example is aluminum which is a common proxy for fine-grained sediments and is a dominate component in aluminosilicate or clay minerals often not affected by diagenesis (Burmsack, 2006; Tribovillard et al., 2006). The correlation

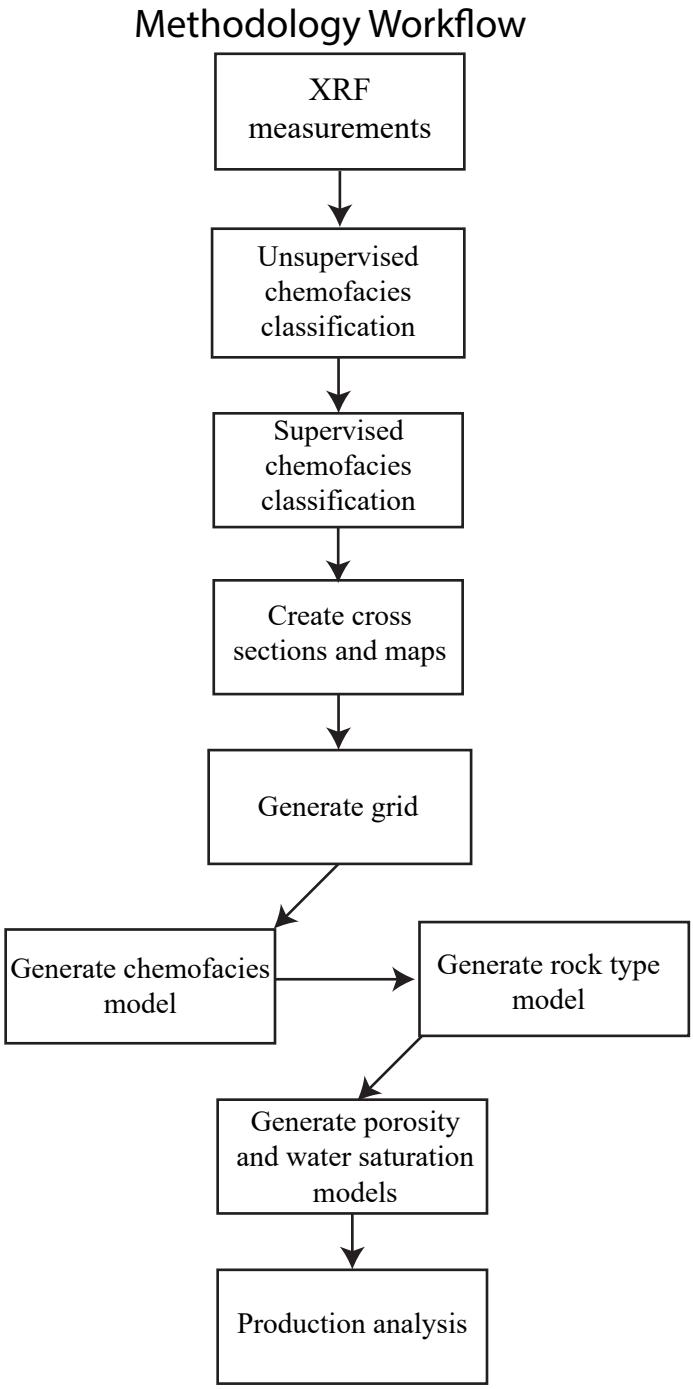

Figure 3: Overall workflow includes defining chemofacies, creating cross sections and maps followed by generating a model grid. Once the grid is created, chemofacies, rock type, and petrophysical models can be generated within that grid. Models can be extracted along the lateral of producing wells to analyze each facies and property against well productivity.

coefficient between aluminum and other elements can be used to determine which elements are associated with clay minerals and grain-size.

Indicator Element Selection

Certain elements (Figure 4) are used as proxies for environmental conditions during deposition (Pearce and Jarvis, 1992). The elements used in this study include titanium (Ti), zirconium (Zr), aluminum (Al), potassium (K), silicon (Si), calcium (Ca), and strontium (Sr). Ti and Zr are useful proxies because they are purely detrital in origin and immobile during diagenesis; however, Ti is also interpreted to be deposited by aeolian processes as it is more likely to be incorporated into minerals that are easily windblown (Bhatia and Crook, 1986; Tribovillard et al., 1994; Sageman and Lyons, 2004). Al and K are used as clay proxies; however, they can also materialize in alkali feldspars (Pearce et al., 1999; Tribovillard et al., 2006). As K and Al concentrations increase while Zr decreases, a more distal depositional environment can be interpreted (Turner, 2016). Si can be associated with both detrital and biogenic quartz as well as clays and feldspars, so by observing Si in a ratio with Al and Ti, silicon can be used as a proxy for biogenic and continentally derived quartz (Pearce and Jarvis, 1992; Pearce et al., 1999; Sageman and Lyons, 2004). When the quartz proxy, Si/Ti ratio is high while Zr, a proxy for detrital sediments, is low, biogenic quartz can be interpreted as an interval of low sedimentation or an algal bloom. Long intervals would indicate prolonged non-deposition allowing the settling of biogenic quartz, whereas short episodes are more indicative of algal blooms (Turner, 2016). Ca and Sr are associated with carbonate source, but are mobile during diagenesis, so multiple proxies must be used in addition to Ca and Sr to fully interpret environmental conditions (Banner, 1995; Tribovillard et al., 2006). By observing the Mg/Ca

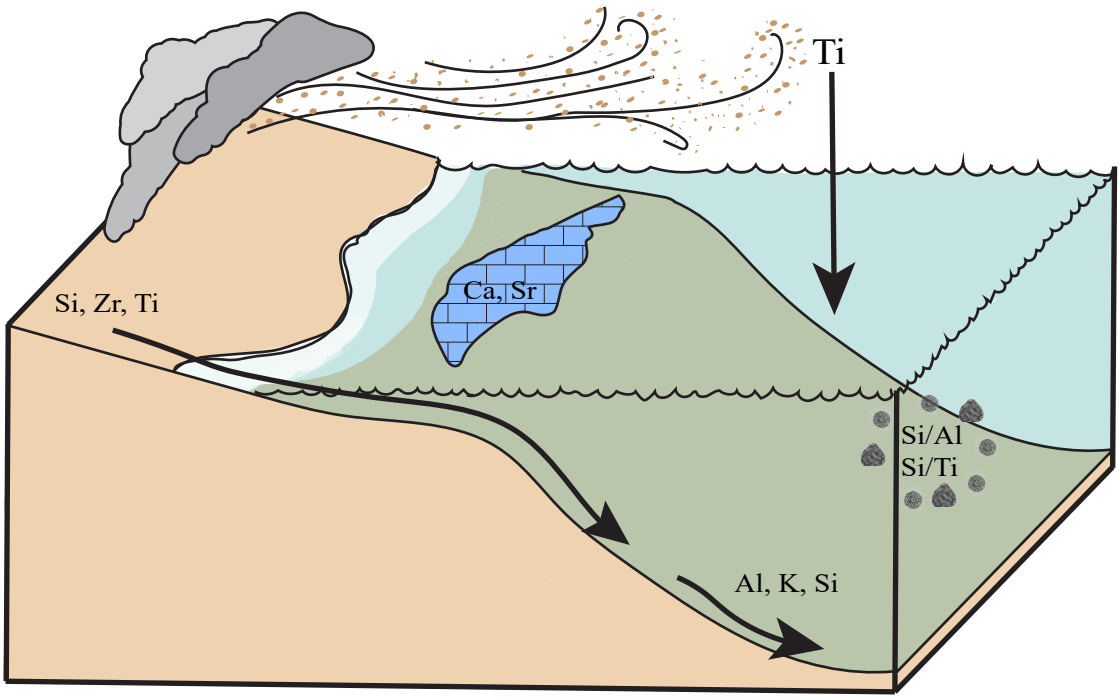

Figure 4: The box diagram above shows a marine environment of where certain elements can be used as proxies for provenance and environmental conditions (Pearce and Jarvis, 1992). This figure illustrates how elements are indicative of those proxies. Ti and Zr are elements that are overwhelmingly detrital in origin and are highly immobile during diagenesis. These elements can flag continentally-sourced sediments. Ti can also be a proxy for aeolian sedimentation, as it often materializes in elements that are easily wind-blown (Bhatia and Crook, 1986; Sageman and Lyons, 2004; Tribovillard et al., 2006). Al and K are used as proxies for clay and can be indicative of a relatively deeper water setting where clay settles in marine environments (Pearce et al., 1999; Tribovillard et al., 2006). Because Si can materialize in clays, feldspars, and is prevalent within both deep water and continentally-sourced settings, it is more useful as a proxy in the form of a ratio with Al and Ti. Si/Al and Si/Ti can be used as proxies for biogenic and continentally-derived quartz (Pearce and Jarvis, 1992; Pearce et al., 1999; Sageman and Lyons, 2004). Ca and Sr are proxies of carbonate source, however they are highly mobile during diagenesis, so other proxies must be used in addition to determine the true source of these elements (Banner, 1995; Tribovillard et al., 2006).

ratio, the type of diagenesis can be determined. During meteoric diagenesis both aragonite and high-magnesium calcite are replaced by low-magnesium calcite (Tucker and Wright, 1990). The geochemistry results in depleted Sr and Mg while iron (Fe) and manganese (Mn) may be enriched as they are often present in groundwater (Benson, 1974; Tucker and Wright, 1990). If the environment of diagenesis is meteoric then Sr/Ca can be used as a proxy of the degree of diagenetic alteration. High Sr/Ca values are interpreted as zones of low diagenesis, while low Sr/Ca values are indicative of high diagenetic alteration. Table 1 summarizes the element proxies used in this study.

K-means Classification

K-means clustering is a method of unsupervised learning used to determine natural clusters in data. Data assignment is the first step of K-means classification. A centroid defines a cluster and each data point is assigned to the nearest centroid based on the squared Eucildean distance, or the distance between centroids (Trevino, 2016). The algorithm reselects centroids and data are reassigned until the proper number of clusters is determined, this occurs when data points no longer change clusters. For the final clusters, the distance between data points within a cluster is minimized and the distance between data points in different clusters is maximized (Kumar and Kishore, 2006). Elbow plots are used to determine the optimal number of clusters within the dataset. These plots display the sum of squared distances between (SSB) and within (SSW) for any number of clusters. The chemofacies data from the Gulf Oil 1-25 Rohling, Gulf Oil 1-23 Shaffer, Well A, Well B, and Well C cores have 3 natural clusters as determined by their elbow plots, but could potentially be divided into more clusters. To ensure each Meramec chemofacies is represented, multiple classifications with varying numbers of clusters was tested.

Element	Proxy	Source
Titanium (Ti), Zirconium (Zr)	Indicator of continentally derived sediments; Titanium can be associated with aeolian sedimentation	Sageman and Lyons, 2004; Tribovillard et al., 2006
Aluminum (Al), Potassium (K)	Primarily associated with clay minerals and fine grained sediments	Sageman and Lyons, 2004; Tribovillard et al., 2006
Silicon/Aluminum (Si/Al), Silicon/Titanium (Si/Ti)	Indicator of detrital and biogenic quartz	Pearce and Jarvis, 1992; Pearce et al., 1999; Tribovillard et al., 2006
Calcium (Ca), Strontium (Sr)	Indicator of carbonates	Banner, 2005; Tribovillared et al., 2006
Strontium/Calcium (Sr/Ca)	Degree of diagenetic alteration	Tucker, 1981; Given and Wilkinson, 1985
Magnesium/Calcium (Mg/Ca)	Detrermine type of cement and associated diagenetic environment	Given and Wilkinson, 1985

Table 1: Indicator elements are chosen to develop and interpret chemofacies based on their proxies to environmental conditions. Above each indicator element is shown with its environmental proxy and the literature source.

The data were classified three separate times into 3, 5 and 7 clusters to ensure the optimal number of clusters was determined.

The average weight percent (wt%) of each element per cluster is divided by the average wt% of that element within the entire core. The output is the average wt% of a given element within each cluster with regard to its overall presence in the core (Appendix-C4). By observing how the wt% of an element varies on average from cluster to cluster, an interpretation can be made about each cluster based on the element environmental proxy. The enrichment (or depletion) of indicator elements within clusters is indicative of environmental conditions based on its proxy.

Random Forest Classification

As discussed, chemofacies are defined through cluster interpretation by K-means unsupervised classification. To interpret the chemostratigraphic framework and evaluate the spatial distribution of chemofacies, chemofacies were classified within non-cored wells. By using a supervised machine-learning technique called Random Forest, chemofacies were classified in non-cored wells based on their relationships with well logs The wells of the cross-sectional model were separated into four geographic areas as shown in Figure 5. The wells within these areas exhibit similar GR, NPHI and RHOB histograms and log signatures to the cored wells in which they are grouped.

Random Forest is a supervised learning technique that is composed of multiple decision trees to arrive at a classification result. Random Forest uses two data sets, a training set and a testing set (for the purpose of this study 60% of the dataset is used as the training set and 40% is the testing set). In addition, data from the five cored wells were used for blind tests to determine

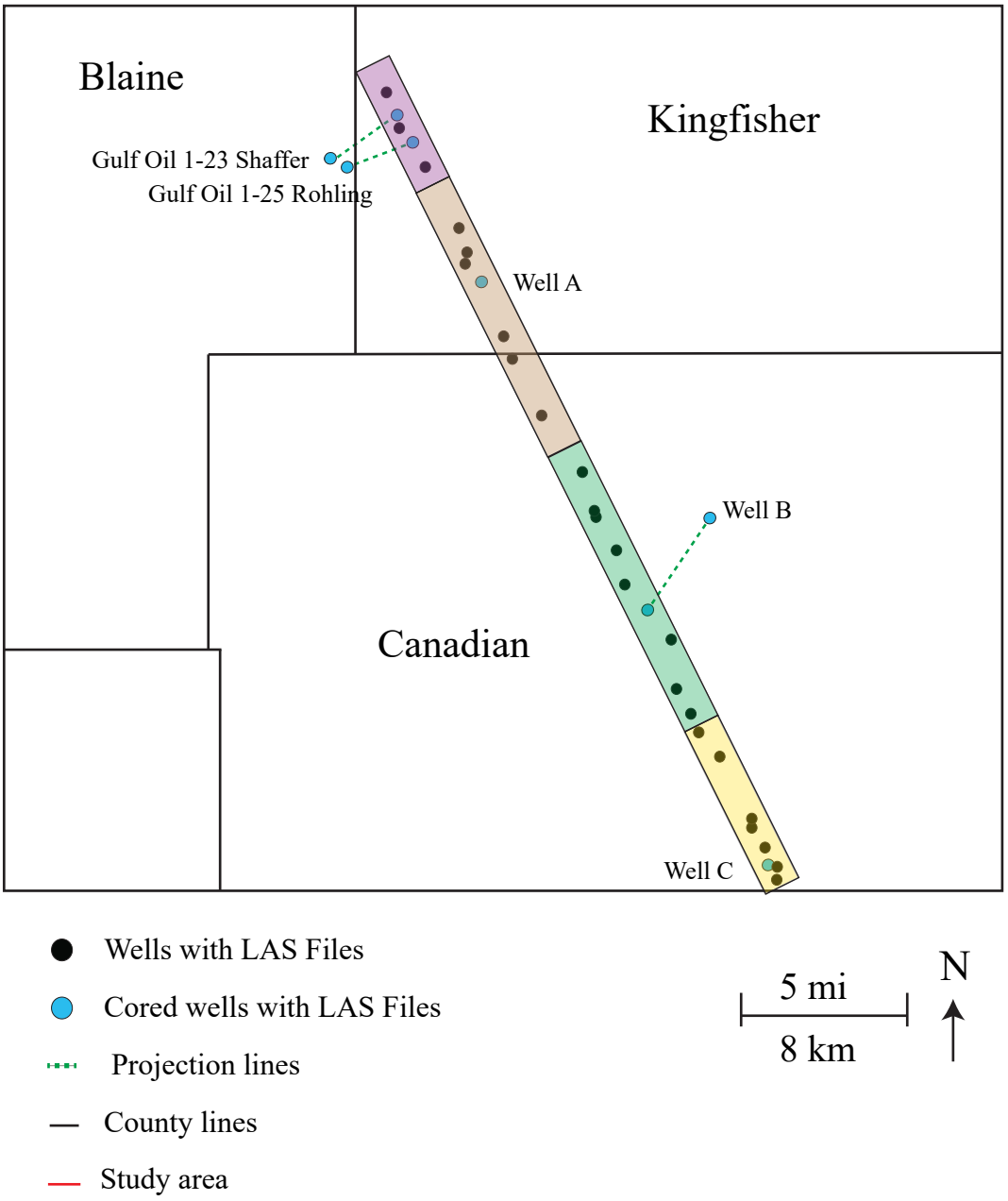

Figure 5: Each cored well (except Gulf Oil 1-23 Shaffer) are used to classify chemofacies logs in non-cored wells that share GR, RHOB and NPHI trends and are geographically close. Due to geologic variation from a proximal to distal setting, each cored well is used to ensure higher prediction accuracies.

the accuracy of the chemofacies classification. To do a blind test on each core, the data were split in half. One half of the data were used to build the Random Forest model that was further divided into a training and testing sets for Random Forest cross validation. The model uses the training set to learn the relationship between the predicting factor (chemofacies), and the data used to predict (well logs), and cross-validates the output predicted chemofacies log to the actual chemofacies log an n amount of times (in this study n=10). By gathering predictive data from each of the decision trees, a prediction output can be determined based on the most common answer of each decision tree and is then cross-validated with the testing data. The well logs used include gamma ray (GR), neutron porosity (NPHI), and bulk density (RHOB). These logs are chosen because they are prevalent throughout the study area. The resulting model was applied to the blind test data, and the predicted chemofacies log was compared to the actual chemofacies log.

Petrophysics

Total porosity, effective porosity, water saturation and reservoir quality logs were calculated in Petrel using core-derived data and normalized well logs including gamma ray (GR), neutron porosity (NPHI), bulk density (RHOB), and deep resistivity (RILD). Total porosity calculations require density porosity logs (DPHI) which were not included in the data and subsequently calculated using RHOB and grain density calculated from core XRF-derived mineralogy (Heyleem Han, 2018, personal communication). Grain densities were determined for each chemofacies by averaging the major minerals within the Meramec: quartz, calcite, dolomite, feldspar and clay. The major minerals were multiplied by that mineral's density and summed to produce an average grain density for each chemofacies. Bulk density logs,

chemofacies logs and the chemofacies' associated grain densities were used to calculate DPHI logs in both cored and non-cored wells.

$$DPHI = \frac{(Grain\ Density - RHOB)}{(Grain\ Density - 1)}$$

Total porosity (Φ_{tot}) is calculated as the root mean square (RMS) of the NPHI log and a calculated DPHI log:

$$\Phi_{tot} = \sqrt{\frac{DPHI^2 + NPHI^2}{2}}.$$

To correct for clay, shale volume (V_{sh}) and effective porosity (Φ_{eff}) are calculated using a normalized gamma ray logs and the average porosity of illite (Φ_{AVGsh}) mineralogy calculated from core XRF-derived mineralogy:

$$V_{sh} = \frac{GR - GR_{min}}{GR_{max} - GR_{min}}, \text{ and}$$

$$\Phi_{eff} = \Phi_{tot} - (V_{sh} * \Phi_{AVGsh}).$$

Water saturation logs are calculated using the Archie equation, deep resistivity logs (RILD), and effective porosity logs (Φ_{eff}). Parameters for Archie's equation were determined through core measurements (Ali Tinni, 2019, personal communication):

$$S_w = \left(\frac{R_w}{\Phi^m R_T}\right)^{\frac{1}{n}},$$

where cementation exponent $|m|$=1.73, the saturation exponent $|n|$ is a function of porosity, and the resistivity of formation water $|Rw|$=0.026 Ohm • m. Also, in this study, reservoir quality indicator (RQ) is used as a qualitative measure of reservoir quality and is calculated using effective porosity, water saturation and gamma ray logs.

$$RQ = \frac{\Phi_{eff}(1 - S_w)}{GR}$$

Stratigraphic Correlation and Reservoir Zonation

Chemofacies logs and conventional wells logs were used to interpret and correlate the Meramec stratigraphy in the study area. Reservoir zones (parasequences) were determined based on the stratigraphic variability of chemofacies. Parasequences were determined based on Ti and Zr trends (elemental proxies for continental sourced sediments). Increasing Ti and Zr content is interpreted as a transgressive zone, decreasing Ti and Zr is indicative of regressive zones. Interpreting cyclicity based on Ti and Zr provides a higher resolution than gamma ray as XRF samples were acquired at a 1-in (2.54-cm) resolution. Ti and Zr are also directly linked to detrital source unlike gamma ray which is a function of clay content and amounts of uranium, thoriaum, and potassium.

Rock-Type Definition

Core-derived porosity and permeability from the Gulf Oil 1-25 Rohling, Gulf Oil 1-23 Shaffer, Well A and Well B were used to define rock types and rock type logs (Ishank Gupta, 2018, personal communication). Flow zone indicator (FZI) cutoffs were applied to cross plots of core-derived porosity and permeability measurements to define rock types. Equations developed by Amaefule et al. (1993) were used to determine parameters to define flow zone indicator cutoffs such as the Resrevoir Quality Index (RQI) and the pore-to-grain volume. (Amaefule et al., 1993):

$$RQI = 0.0314 * \sqrt{\frac{k}{\Phi}},$$

$$R_{pvgv} = \frac{\Phi}{1-\Phi},$$

$$FZI = \frac{RQI}{R_{pvgv}}$$

Where:

k = permeability (air)

Φ = porosity

R_{pvgv} = pore-to-grain volume ratio

RQI = Reservoir Quality Index

FZI = Flow Zone Indicator

Once initial flow zone indicator cutoff values are determined, petrophysical and geomechanical properties were analyzed for each rock type and cutoffs are adjusted until each rock type was associated with contrasting petrophysical and geomechanical properties (Ishank Gupta, 2018, personal communication).

Reservoir Modeling

Chemofacies logs, stratigraphic correlations, rock type classifications and calculated petrophysical logs were integrated to produce dip-oriented, proximal to distal reservoir models from southern Kingfisher County to southern Canadian County. The model was constrained to 24 non-cored wells and 5 cored wells. Cored wells including the Gulf Oil 1-23 Shaffer, Gulf Oil 1-25 Rohling and Well B were projected into the model domain (approximately parallel to contours of a regional Meramec structure map (Katie Drummond, 2018, personal communication). A 3-D model grid was generated to represent the Meramec stratigraphic framework. Surfaces and isopach maps for the Woodford, Osage, and Meramec parasequences 1-7 were created to represent 8 model zones. The zones were made with a proportional layering

scheme with a mean layer thickness of 2 ft (0.61 m). For the cross-sectional model, cell lateral dimensions parallel to the cross section are 100 ft (30.5 m) and the grid was rotated 26.3° such that the model cross-section is oriented along the trend of deposition from northwest to southeast (Figure 6). The width of the cross-sectional model was arbitrarily set to 8,600 ft (2,621.3 m). The resulting grid has 43 x 2044 x 251 cells in I, J, and K directions, and 22,060,892 cells.

Chemofacies logs were upscaled to the model grid such that the most abundant chemofacies within each cell was assigned to that cell. Sequential-indicator simulation (SIS) was used to model chemofacies. The spatial correlation of these parameters was quantified with distance and direction using variography. Vertical chemofacies variograms were generated for each Meramec zone and each chemofacies and were interpreted using normal and nested spherical variogram models. For each variogram, the nugget was set to zero to honor all the upscaled chemofacies logs. Because the scale of lateral reservoir heterogeneity within the Meramec is commonly less than the well spacing and cannot be properly represented by experimental horizontal variograms, horizontal chemofacies variogram parameters for the major and minor directions were estimated and used for each chemofacies within each zone. The azimuth for the major horizontal chemofacies variogram was set to -27° N to match the major direction of the grid which trends from northwest to southeast. The variogram ranges and chemofacies percentages are summarized in Appendix-E2. The spatial distribution of chemofacies is constrained by chemofacies log data and chemofacies proportion volumes. Chemofacies proportion volumes are created by generating chemofacies vertical proportion curves for each of the four geographic zones that were divided for the classification of chemofacies. The vertical proportion curve log data were mapped to generate a proportion volume for each of the three chemofacies.

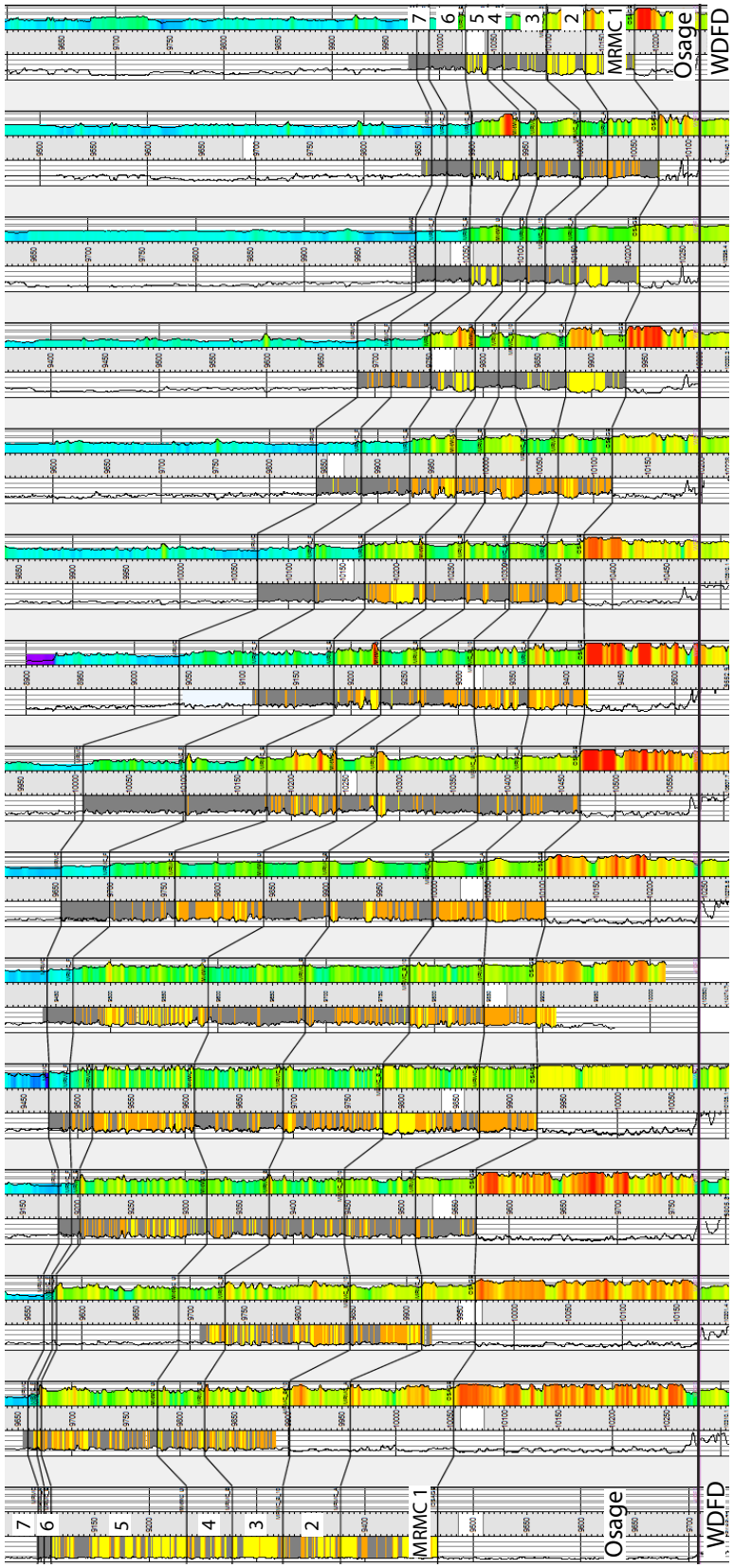

Figure 6: The cross section above shows the zones of the Meramec that were included in the reservoir model. Parasequences of the Meramec were picked based on chemofacies stacking patterns, gamma ray trends and resistivity logs. The cross section shows an overall thinning of the Meramec from the northwest to the southeast. The cross section is flattened on the Woodford Shale.

Rock type logs were upscaled to the model grid such that the most abundant rock type within each cell was assigned to that cell. Because each chemofacies is associated with the abundance of a specific rock type, the rock type logs were upscaled using a bias to the chemofacies model. Rock types were modeled using sequential-indicator simulation (SIS). Nested and normal variogram models were used to quantify rock type variation with distance and direction. The nugget was set to zero to honor all upscaled rock type logs. Experimental horizontal rock type variograms were used to estimate variation for the major and minor horizontal directions. Due to a range of rock types existing within each chemofacies, horizontal ranges for the major and minor directions were estimated to be slightly less than the ranges used in the chemofacies modeling. The azimuth for the major direction was set to match that of the grid that trends from the northwest to southeast.

Effective porosity, water saturation and reservoir quality logs were upscaled to the model grid assigning each cell the arithmetic mean and biased to the chemofacies model. Effective porosity, water saturation and reservoir quality were modeled using sequential-Gaussian simulation (SGS) and constrained to the chemofacies model. SGS is a variogram-based modeling technique similar to SIS which was used to model chemofacies and rock types. Normal spherical vertical variogram ranges were determined to quantify variance with distance and direction. Experimental horizontal variogram ranges were determined to be less than that of the rock types and the chemofacies, as there is a range of values for porosity, water saturation and reservoir quality associated with each rock type and chemofacies.

Production Analysis

To determine drivers for production, 60-, 90- and 120-day cumulative oil production data were used to compare to chemofacies, rock types, porosity, and water saturation based onthe reservoir models. Chemofacies distribution along the lateral of five producing wells was extracted from the chemofacies model to compare to oil production. Effective porosity and reservoir quality were averaged from extracted logs from the property models. Water saturation, S_w, distribution along the lateral was averaged by calculating the total water volume divided by the total pore space rather than averaging water saturation at each depth:

$$\overline{Sw} = \frac{\sum(S_w \Phi h)}{\sum \Phi h},$$

where h represents the depth increment along the lateral. Data identified along the horizontal portion of the well was determined by selecting log data from depths that have an inclination of 75° and higher.

RESULTS

Meramec chemofacies

The Meramec consists of three natural clusters with varying element content that were defined using K-means classification for the Gulf Oil 1-25 Rohling, Gulf Oil 1-23 Shaffer, Well A, Well B, and Well C cored wells. The elbow plot results (Figure 7) illustrate the sum of squared distances within and between 3 clusters is optimal. Sum of squared distances within and between cluster numbers beyond 3 show less variation and could result in difficulty distinguishing one cluster from another, but 5 and 7 clusters were classified to ensure that theory based on the elbow plot's results.

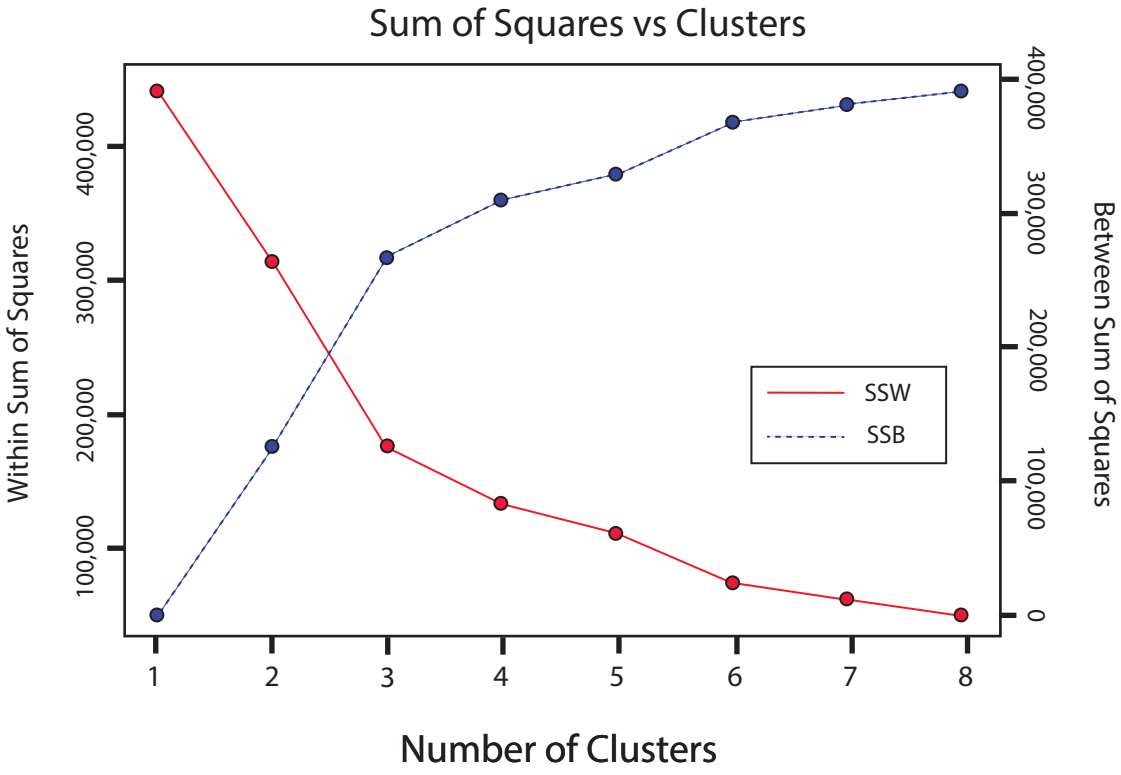

Figure 7: The elbow plot above shows the sum of squared distances between and within each cluster for each number of clusters that can be chosen for the classification. Where the sum of squared distances within and between vary the most, the optimal number of clusters can be determined. Above is the elbow plot from Well A which indicates that 3 clusters is the optimal number of clusters within the data.

The classification results for 5 clusters and 7 clusters exhibited a sufficient amount of overlap in element distributions, and produced clusters that had no geologic meaning. When the data were classified into 3 clusters, each cluster represented an independent chemofacies that had varying elemental distributions within each cluster and sufficiently contrasted with each other. The final K-means classification produced 3 clusters to be interpreted based on the elemental distributions within each cluster to define chemofacies (Figure 8).

Cluster 1, interpreted as a calcareous sandstone, has a relatively high silicon (Si) to aluminum (Al) ratio (Si/Al) which is indicative of terrestrial and biogenic quartz, as well as relatively high concentrations of calcium (Ca) and strontium (Sr), which are indicative of a carbonate source. The calcareous sandstone has intermediate concentrations of titanium (Ti) and zirconium (Zr) both of which are highly immobile and primarily terrestrial in origin (Tribovillard et al., 1994) and indicate sediments from a detrital source. The quartz in the calcareous sandstone chemofacies is likely a mix of terrestrial-derived and biogenic quartz considering the intermediate concentrations of terrestrial derived proxies and very low concentrations of aluminum (Al) and potassium (K), which are indicative of clays. The calcareous sandstone also has a low average value of strontium (Sr) to calcium (Ca) ratio (Sr/Ca) indicating this cluster is diagenetically altered to a relatively high degree.

Cluster 2, interpreted as the argillaceous-calcareous siltstone, is composed of intermediate concentrations of each indicator element with slightly higher Ca and Sr concentrations and a low Sr/Ca ratio, and is likely a transitional chemofacies with a high degree of diagenetic alteration.

Cluster 3, interpreted as a detrital mudstone chemofacies, is composed of high concentrations of Al, K, Ti and Zr, indicating high clay content that is continentally sourced and

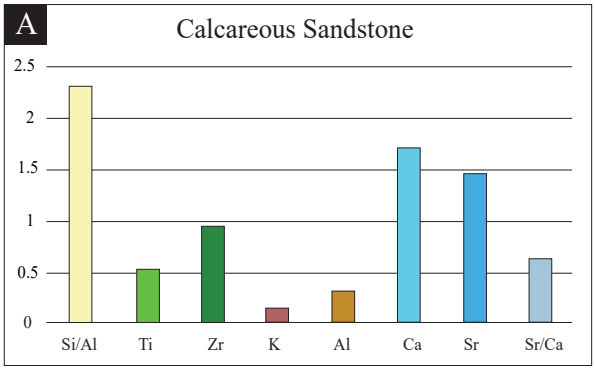
A
Calcareous Sandstone
2.5
2
1.5
1
0.5
0
Si/Al
Ti
Zr
K
Al
Ca
Sr
Sr/Ca

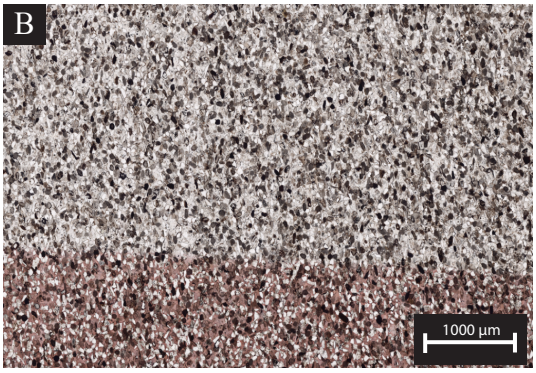
B
1000 µm

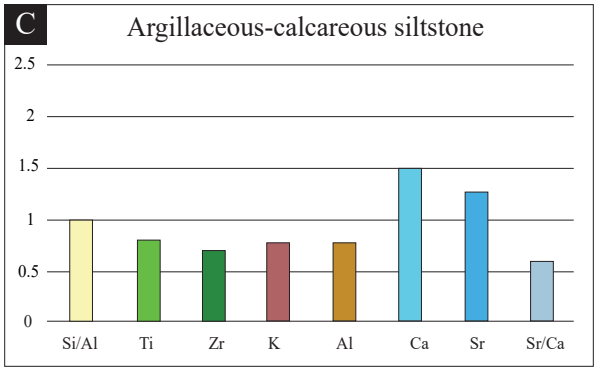
C
Argillaceous-calcareous siltstone
2.5
2
1.5
1
0.5
0
Si/Al
Ti
Zr
K
Al
Ca
Sr
Sr/Ca

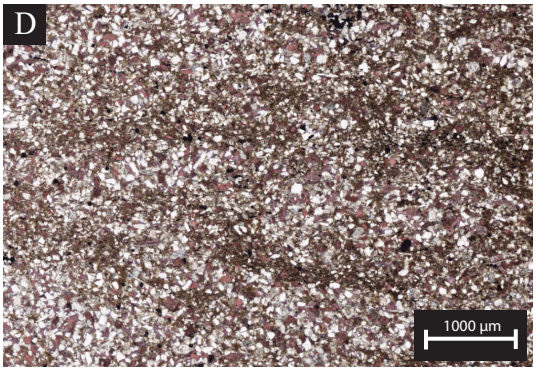
D
1000 µm

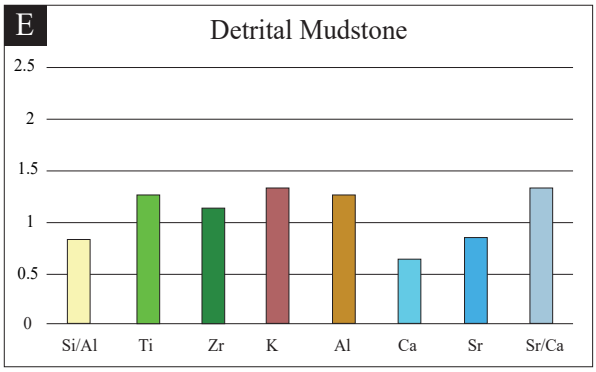
E
Detrital Mudstone
2.5
2
1.5
1
0.5
0
Si/Al
Ti
Zr
K
Al
Ca
Sr
Sr/Ca

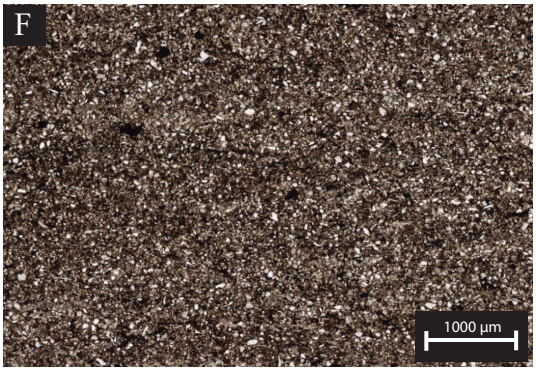
F
1000 µm

Figure 8: The Meramec is composed of 3 chemofacies: calcareous sandstone, argillaceous-calcareous siltstone and detrital mudstone. Thin section images are shown next to the bar chart showing the average element weight percentages within each chemofacies (calculation shown in Appendix-C4). The logs at the base of each chemofacies descriptions shows where those thin sections are located within the Meramec. The calcareous sandstone is composed of high Si/Al indicating mixed biogenic and detrital sourced quartz. The calcareous sandstone has high Ca and Sr with low Sr/Ca indicative of high diagenetic alteration. The argillaceous-calcareous siltstone has moderate levels of Si/Al, Ti, Zr, K and Al indicating moderate detrital-sourced quartz and clay volume. This chemofacies has high levels of Ca and Sr with a low Sr/Ca indicating high diagenetic alteration. The detrital mudstone chemofacies has high levels of Ti, Zr, K, and Al indicating a continentally-sourced clay rich facies. Moderate Si/Al levels indicate moderate quartz volume. Low Ca and Sr along with a high Sr/Ca ratio indicates low carbonate source and diagenetic alteration.

moderate quartz proxies that correlate with Zr, indicating the quartz is predominately detrital within this chemofacies. The detrital mudstone has low Ca and Sr values indicating a low carbonate source. The Sr/Ca ratio is high in the detrital mudstone, indicating relatively low degree of diagenetic alteration.

The K-means classification resulted in a chemofacies log for the Meramec for each of the cored wells illustrated in Figure 9 alongside indicator element profiles and the gamma ray log. The chemofacies descriptions are shown in Table 2.

Chemofacies classification in non-cored wells

Chemofacies are classified in 24 non-cored wells using a supervised machine learning technique, Random Forest. The cored wells resulted in up to 83% overall accuracy for the blind tests for classifying chemofacies (Figure 10). Confusion matrices of the cross validation from Random Forest is shown in Table 3 for the Gulf Oil 1-23 Shaffer, Gulf Oil 1-25 Rohling, Well A, Well B and Well C. The blind test for the Gulf Oil 1-23 Shaffer resulted in 49 % overall accuracy for predicting chemofacies. The blind test for the Gulf Oil 1-25 Rohling resulted in 55 % overall accuracy for predicting chemofacies. The blind test for Well A resulted in 75 % overall accuracy, Well B resulted in 77 % overall accuracy and Well C resulted in 83 % overall accuracy from their blind tests. Each core, with the exception of the Gulf Oil 1-23 Shaffer, a core with relatively low overall accuracy, was used to predict chemofacies logs in non-cored wells.

Meramec chemostratigraphy

The Meramec stratigraphy is interpreted to consist of seven upward-shallowing parasequences (Figure 11) that are capped by marine-flooding surfaces (in ascending order,

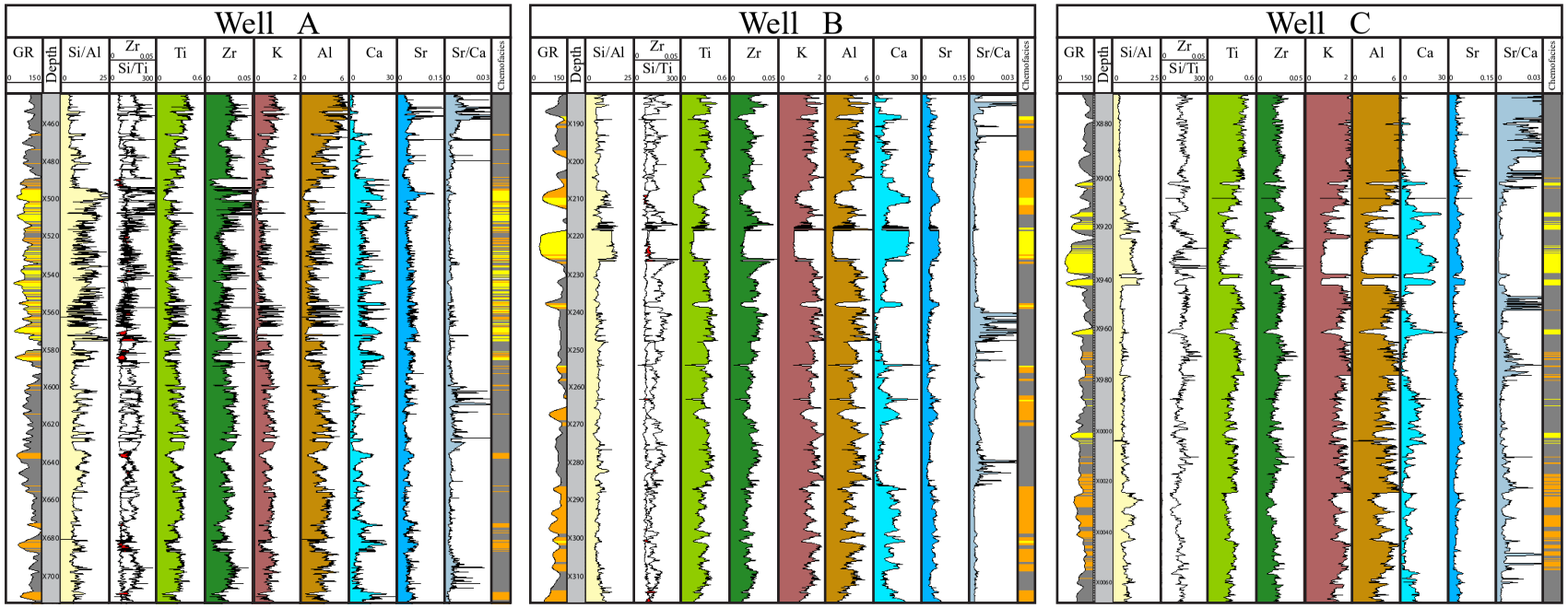

Figure 9: Gamma ray and elemental profiles from XRF for Well A, Well B and Well C. The final track exhibits the resulting Chemofacies log from the K-means classification and is used as the color fill for the gamma ray. The element profiles show the stratigraphic variation of each element's weight percent throughout the Meramec.

Chemofacies	Description	Depositional Setting
Detirtal mudstone	Comprised of high concentrations of Al, K, Ti and Zr indicating high clay content that is continentally sourced. Moderate levels of Si/Ti and Si/Al that correlate to Zr indicating detrital quartz. Low Ca and Sr and high Sr/Ca indicating low carbonate source and low degree of diagenetic alteration	Distal Marine
Argillaceous calcareous siltstone	Composed of moderate concentrations of each indicator element;. transitional chemofacies. Moderate amount of detrital quartz, clay, and calcite cement. Low concentrations of Sr/Ca indicate very high diagenetic alteration.	Mid-ramp; transition zone
Calcareous sandstone	Comprised of high concentrations of Si/Al, Ca, and Sr, indicative of carbonate, detrital and biogenic quartz. Intermediate concentrations of Ti and Zr indicate sediments are mixed detrital and carbonate/biogenic source. Very low concentrations of Al and K indicate little clay content. Low Sr/Ca ratio indicates high diagenetic alteration.	Inner ramp; within wave base

Table 2: The Meramec is comprised of 3 chemofacies including the detrital mudstone, argillaceous-calcareous siltstone and calcareous sandstone. Above, there is a detailed description of element distribution of each chemofacies and their proxies. To the right, the depositional setting is interpreted for each chemofacies.

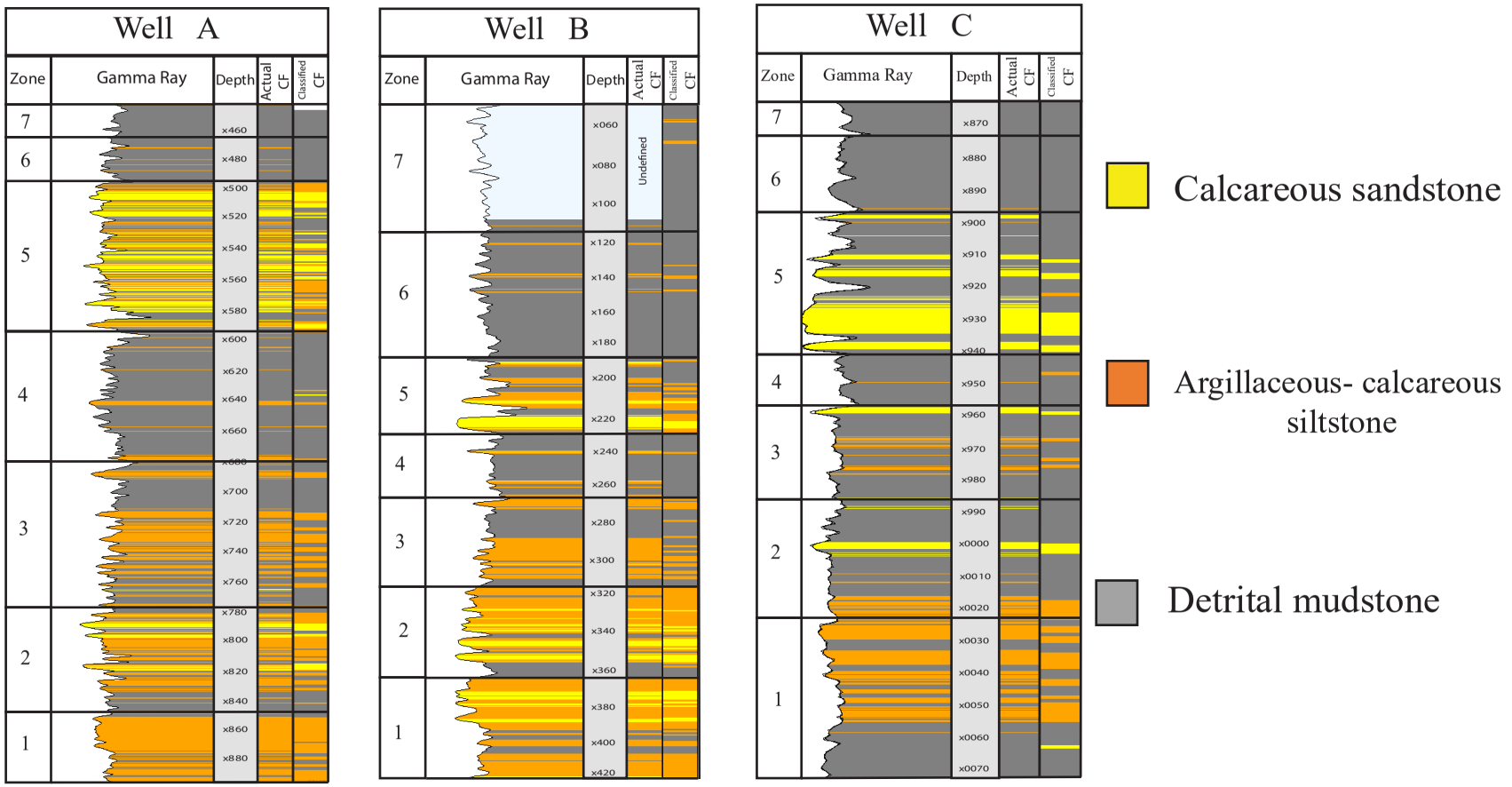

Figure 10: Log data from Wells A, B and C were divided into two halves both of which are representative of this distributions of chemofacies. One half was used to build a Random Forest model and was further divided into a training set and testing set for cross validation. That model was then applied to the second half of the original data set for a blind test. The artificial chemofacies log from that blind test is shown on the far right track. The actual chemofacies log is shown on the left track. This blind test proved to be **75, 77, and 83% accuracy** when evaluated through a confusion matrix.

A

ANN / Core	GR, NPHI, RHOB		
	Calcareous sandstone	Arg. Cal. siltstone	Detital mudstone
Calcareous sandstone	29	13	9
Arg. Cal. siltstone	12	98	32
Detital mudstone	8	40	222
User Accuracy	59.2%	64.9%	84.4%

Overall Accuracy: 75.3 %

B

ANN / Core	GR, NPHI, RHOB		
	Calcareous sandstone	Arg. Cal. siltstone	Detital mudstone
Calcareous sandstone	25	12	1
Arg. Cal. siltstone	11	79	23
Detital mudstone	2	25	147
User Accuracy	65.8%	68.1%	86.0%

Overall Accuracy: 77.2 %

C

ANN / Core	GR, NPHI, RHOB		
	Calcareous sandstone	Arg. Cal. siltstone	Detital mudstone
Calcareous sandstone	17	0	4
Arg. Cal. siltstone	0	18	11
Detital mudstone	13	11	151
User Accuracy	56.7%	62.1%	91.0%

Overall Accuracy: 82.6 %

D

ANN / Core	GR, NPHI, RHOB		
	Calcareous sandstone	Arg. Cal. siltstone	Detital mudstone
Calcareous sandstone	16	16	5
Arg. Cal. siltstone	8	45	23
Detital mudstone	11	34	57
User Accuracy	45.7%	47.4%	67.1%

Overall Accuracy: 54.9 %

E

ANN / Core	GR, NPHI, RHOB		
	Calcareous sandstone	Arg. Cal. siltstone	Detital mudstone
Calcareous sandstone	13	7	11
Arg. Cal. siltstone	11	39	42
Detital mudstone	19	27	59
User Accuracy	30.2%	53.4%	52.7%

Overall Accuracy: 48.7

Table 3: A blind test was completed on all 5 cored wells to determine how well chemofacies are predicted based on GR, RHOB, and NPHI well logs. Confusion matrices for each cored well's blind test is shown. A) shows the overall accuracy for well A to be 75.3%. B) Well B has an overall accuracy of 77.2% for predicting chemofacies based on the blind test. C) The overall accuracy for the blind test in well C is 82.6%. D) Gulf Oil 1-25 Rohling blind test resulted in 54.9% overall accuracy and Gulf Oil 1-23 Shaffer blind test resulted in 48.7% being the least accurate for chemofacies prediction. All wells excluding Gulf Oil 1-23 Shaffer were used for generating artificial chemofacies logs in non-cored wells using GR, RHOB and NPHI well logs.

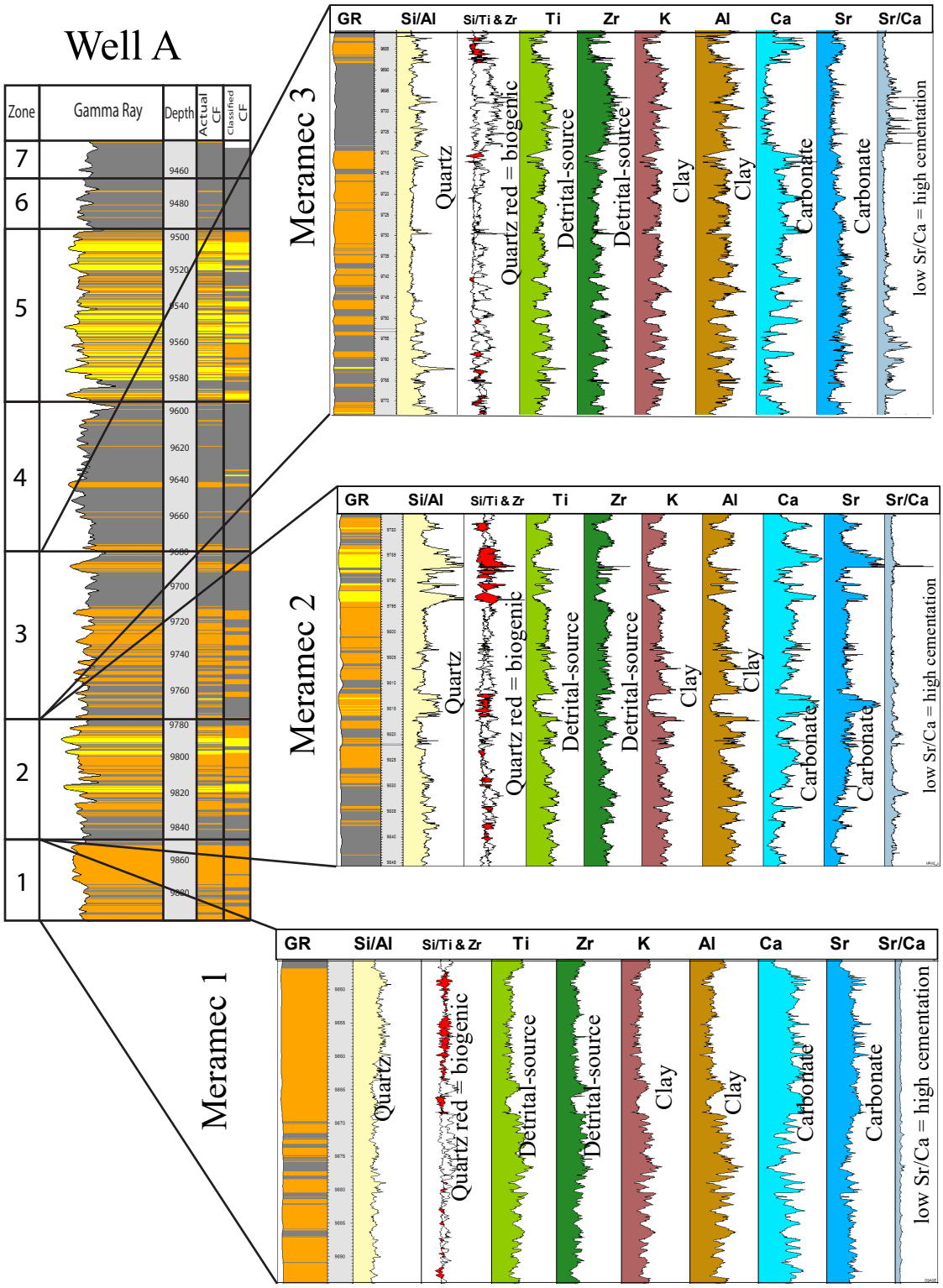
Well A
Zone
Gamma Ray
Depth
Actual CF
Classified CF
7
6
5
4
3
2
1
9460
9480
9500
9520
9540
9560
9580
9600
9620
9640
9660
9680
9700
9720
9740
9760
9780
9800
9820
9840
9860
9880
Meramec 3
Meramec 2
Meramec 1
GR
Si/Al
Si/Ti & Zr
Ti
Zr
K
Al
Ca
Sr
Sr/Ca
Quartz
Quartz red = biogenic
Quartz red ± biogenic
Detrital-source
Clay
Carbonate
low Sr/Ca = high cementation

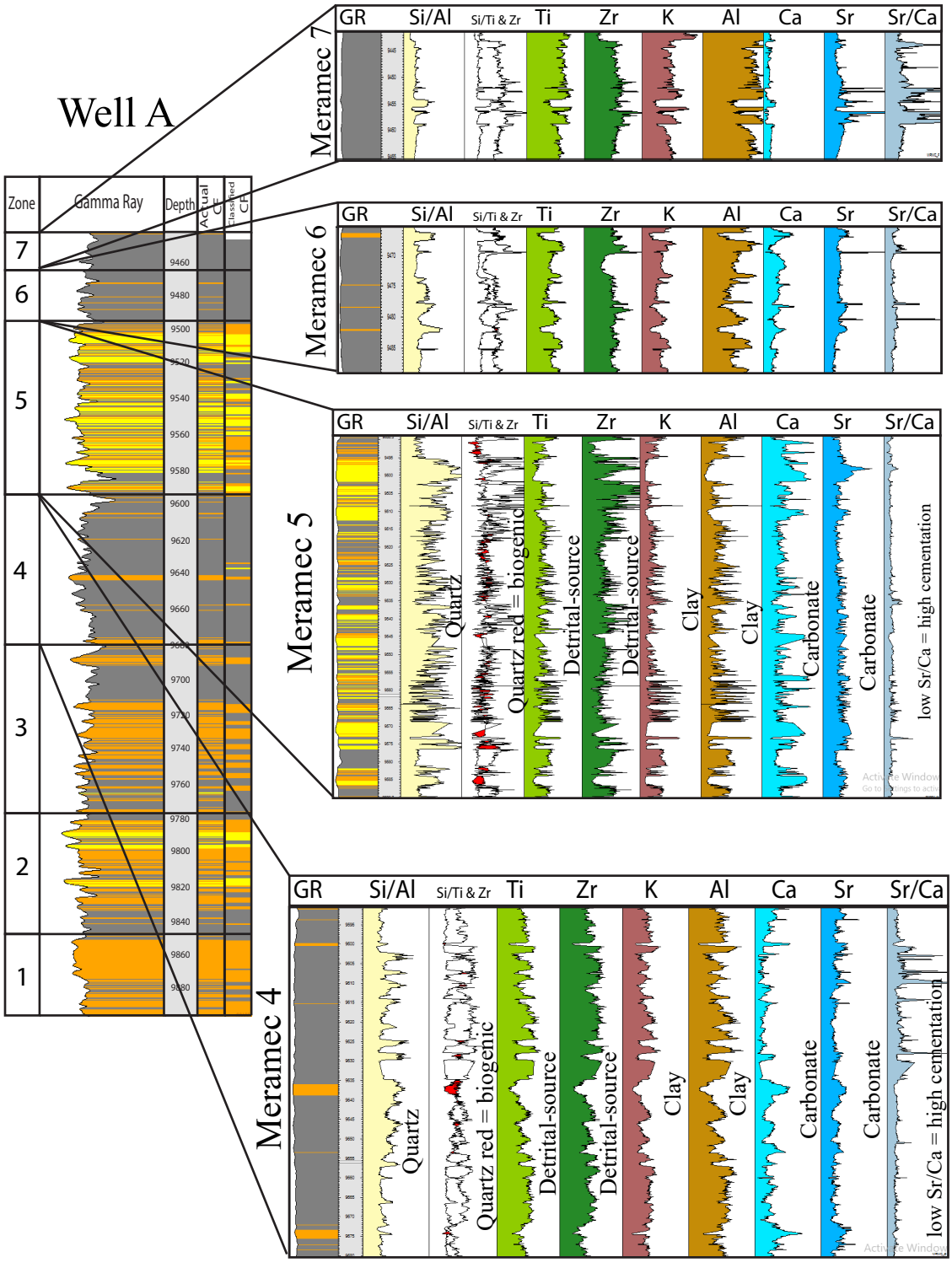
Well A
Zone
Gamma Ray
Depth
Actual CF
Classified CF
7
6
5
4
3
2
1
9460
9480
9500
9520
9540
9560
9580
9600
9620
9640
9660
9700
9740
9760
9780
9800
9820
9840
9860
9880
Meramec 7
Meramec 6
Meramec 5
Meramec 4
GR
Si/Al
Si/Ti & Zr
Ti
Zr
K
Al
Ca
Sr
Sr/Ca
Quartz
Quartz red = biogenic
Detrital-source
Detrital-source
Clay
Clay
Carbonate
Carbonate
low Sr/Ca = high cementation

Figure 11: The chemostratigraphic profiles of Well A are shown to illustrate that stratigraphic variation of elemental proxies and understand the distribution of those proxies within each chemofacies. The Meramec 1 shows increasing quartz proxy (Si/Al) concentration in this zone as well as carbonate proxies (Ca and Sr) and decreasing concentration of detrital sourced clay proxies (K and Al). The diagenetic proxy (Sr/Ca) appears to be consistent throughout. Meramec 2 chemostratigraphic profiles are characterized by increasing quartz proxy (Si/Al) and carbonate (Ca and Sr) source proxies with decreasing Sr/Ca indicating an increase of diagenetic alteration as chemofacies transition from detrital mudstone to interbedded argillaceous-calcareous siltstone and calcareous sandstone. Within the Meramec 3 there is a substantial amount of clay proxies (Al and K) as well as continentally sourced proxies (Ti and Zr) and quartz proxy (Si/Al) towards the top and bottom. Those concentration relationships indicate increasingly detrital sourced clay and quartz. Low concentrations of Si/Al associated with the argillaceous-calcareous siltstone chemofacies indicate less biogenic quartz throughout this parasequence. Low GR response associated with the argillaceous-calcareous siltstone is likely due to the high concentrations of Ca and Sr, which by comparing to the low response of the Sr/Ca proxy, are associated with high cementation in the argillaceous-calcareous siltstone facies that persist in the Meramec 3. The quartz (Si/Al) in the Meramec 3 is associated with the detrital mudstone chemofacies and has a similar trend to Ti and Zr indicating this quartz is continentally derived. The Meramec 4 is dominated by detrital mudstone chemofacies and the chemostratigraphic profiles show moderate to high concentrations of clay proxies (Al and K), continentally derived proxies (Ti and Zr) and quartz proxy (Si/Al) indicating detrital sourced clay and quartz throughout. The Meramec 4 is represented by detrital mudstone chemofacies with small beds of argillaceous-calcareous siltstone most of which disappear with upscaling. There are also many peaks of the diagenetic proxy (Sr/Ca) within the Meramec 4 as compared to the other parasequences indicating the Meramec 4 has the least amount of calcite cement. The Meramec 5 is dominated by the calcareous sandstone chemofacies and has a uniformly low distribution of Sr/Ca ratio, indicating the Meramec 5 is a highly cemented parasequence. At the base of the Meramec 5 there is a section of high Si/Al and Si/Ti and low Zr suggesting the quartz is biogenic in origin. Towards the top of the Meramec 5 the Si/Al and Si/Ti ratios begin to correlate with Zr more consistently indicating an increasingly terrestrial quartz input. Although there are specific points within the Meramec 5 where quartz can be identified as either biogenic or detrital, the majority of the quartz in this parasequence is likely a mixture of both. The mixture of quartz sources combined with the low concentrations of clay proxies (Al and K) can indicate that this zone is prone to quartz cement as well as calcite cement.

named 1 through 7). The stacking patterns of chemofacies in Meramec parasequences are generally represented as detrital mudstones, argillaceous-calcareous siltstones and calcareous sandstones from the base to the top. Parasequences are identified using chemofacies stacking patterns in tandem with Ti and Zr concentrations decreasing upward, topped by a spike of these continentally derived element proxies, representative of a flooding surface.

Meramec 1 is a coarsening upward succession going from interbedded argillaceous-calcareous siltstone and calcareous sandstone to a thick interval of argillaceous-calcareous siltstone. There is increasing quartz proxy (Si/Al) concentration in this zone as well as carbonate proxies (Ca and Sr) and decreasing concentration of detrital sourced clay proxies (K and Al). The diagenetic proxy (Sr/Ca) appears to be consistent throughout this first zone.

Meramec 2 is another coarsening upward sequence starting with a large concentration of detrital mudstone chemofacies at the base coarsening up to interbedded argillaceous-calcareous siltstone and calcareous sandstone. The chemostratigraphic profiles are characterized by increasing quartz proxy (Si/Al) and carbonate (Ca and Sr) source proxies with decreasing Sr/Ca indicating an increase of diagenetic alteration as chemofacies transition from detrital mudstone to interbedded argillaceous-calcareous siltstone and calcareous sandstone.

The Meramec 3 displays two coarsening upward chemofacies sucessions with interbedded argillaceous-calcareous siltstone and detrital mudstone. There is a substantial amount of clay proxies (Al and K) as well as continentally sourced proxies (Ti and Zr) and quartz proxy (Si/Al) towards the top and bottom of the Meramec 3. Those concentration relationships indicate increasingly detrital sourced clay and quartz. Low concentrations of Si/Al associated with the argillaceous-calcareous siltstone chemofacies indicate less biogenic quartz throughout this parasequence. Low GR response associated with the argillaceous-calcareous

siltstone is likely due to the high concentrations of Ca and Sr, which by comparing to the low response of the Sr/Ca proxy, are associated with high cementation in the argillaceous-calcareous siltstone facies that persist in the Meramec 3. The quartz (Si/Al) in the Meramec 3 is associated with the detrital mudstone chemofacies and has a similar trend to Ti and Zr indicating this quartz is continentally derived.

Meramec 4 is dominated by detrital mudstone chemofacies and the chemostratigraphic profiles show moderate to high concentrations of clay proxies (Al and K), continentally derived proxies (Ti and Zr) and quartz proxy (Si/Al) indicating detrital sourced clay and quartz throughout. Meramec 4 is represented by detrital mudstone chemofacies with small beds of argillaceous-calcareous siltstone most of which disappear with upscaling. There are also many peaks of the diagenetic proxy (Sr/Ca) within the Meramec 4 as compared to the other parasequences indicating the Meramec 4 has the least amount of calcite cement.

Meramec 5 is dominated by the calcareous sandstone chemofacies and has a uniformly low distribution of Sr/Ca ratio, indicating the Meramec 5 is a highly cemented parasequence. At the base of the Meramec 5 there is a section of high Si/Al and Si/Ti and low Zr suggesting the quartz is biogenic in origin. This section in the core visually appears to have many white specks. From the elemental data and the core observations it is interpreted that these specks are radiolarian fossils. Toward the top of the Meramec 5 the Si/Al and Si/Ti ratios begin to correlate with Zr more consistently indicating an increasingly terrestrial quartz input. This is consistent with the sequence-stratigraphic interpretation in which the base of the Meramec 5 marks the start of a progradational period. Although there are specific points within the Meramec 5 where quartz can be identified as either biogenic or detrital, the majority of the quartz in this parasequence is likely a mixture of both. The mixture of quartz sources combined with the low

concentrations of clay proxies (Al and K) can indicate that this zone is prone to quartz cement as well as calcite cement.

Meramec 6 is dominated by the detrital mudstone chemofacies, with sparse layers of the argillaceous-calcareous siltstone chemofacies. There is an increasing upward trend of clay proxies (Al and K), detrital source and aeolian proxy (Ti), and carbonate source proxy (Ca) while detrital source proxy Zr and quartz proxy Si/Al exhibits a decreasing trend. Because of the increasing Ti and decreasing Zr concentrations, it is interpreted that the clay input is transported by aeolian sedimentation.

Meramec 7 is dominated by the detrital mudstone chemofacies. This parasequence is represented by significant increases in clay proxies (Al and K) and Ti, indicating aeolian-derived clay input similar to the Meramec 7. There is also very high Sr/Ca indicating low diagenetic cementation. Low concentrations of Si/Al indicate very little quartz within the Meramec 6 and 7, and the high separation of Si/Ti and Zr indicate what quartz does occur in these parasequences is continentally derived.

Stratigraphic variability of chemofacies

Chemofacies model constraints include 1) Meramec stratigraphic framework (3D grid), 2) upscaled chemofacies logs, 3) chemofacies percentages for each zone, 4) variogram parameters for each chemofacies within each zone, and 5) chemofacies proportion volumes.

The stratigraphic variability of chemofacies aligns with the transgressive-regressive-transgressive cyclicity of the Meramec sequence-stratigraphic framework (Figure 12). The chemofacies model (Figure 13a) shows backstepping of chemofacies for Meramec 1 through Meramec 3 with a corresponding overall increase of abundance in detrital mudstone (35 % to 60

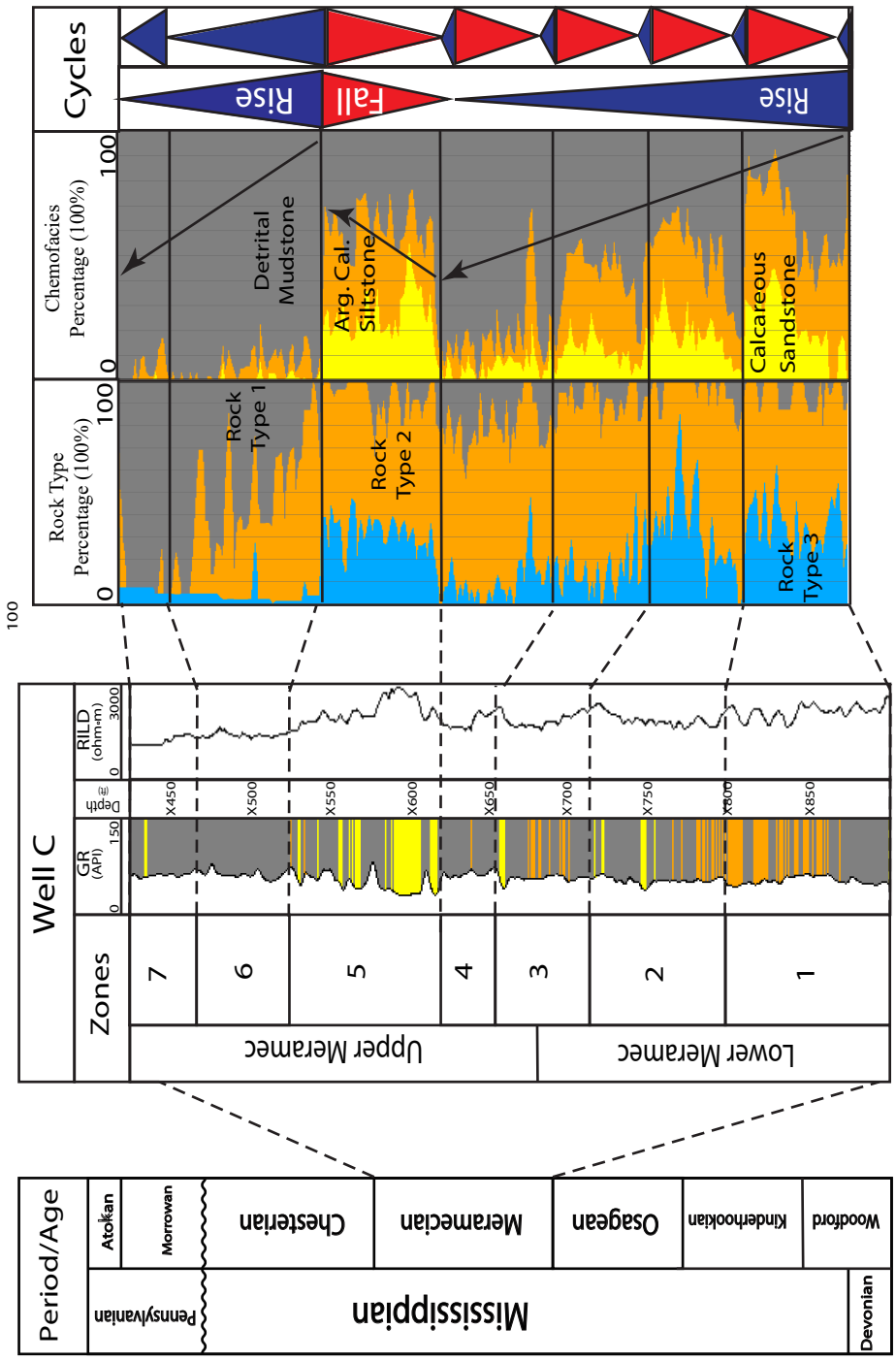

Figure 12: A stratigraphic column of the Mississippian is shown tied to Well C, a cored well in the study area. Meramec interpreted parasequences 1-7 are displayed on the type log and tied to rock type and chemofacies vertical proportion curves to display stratigraphic variability of rock types and chemofacies.

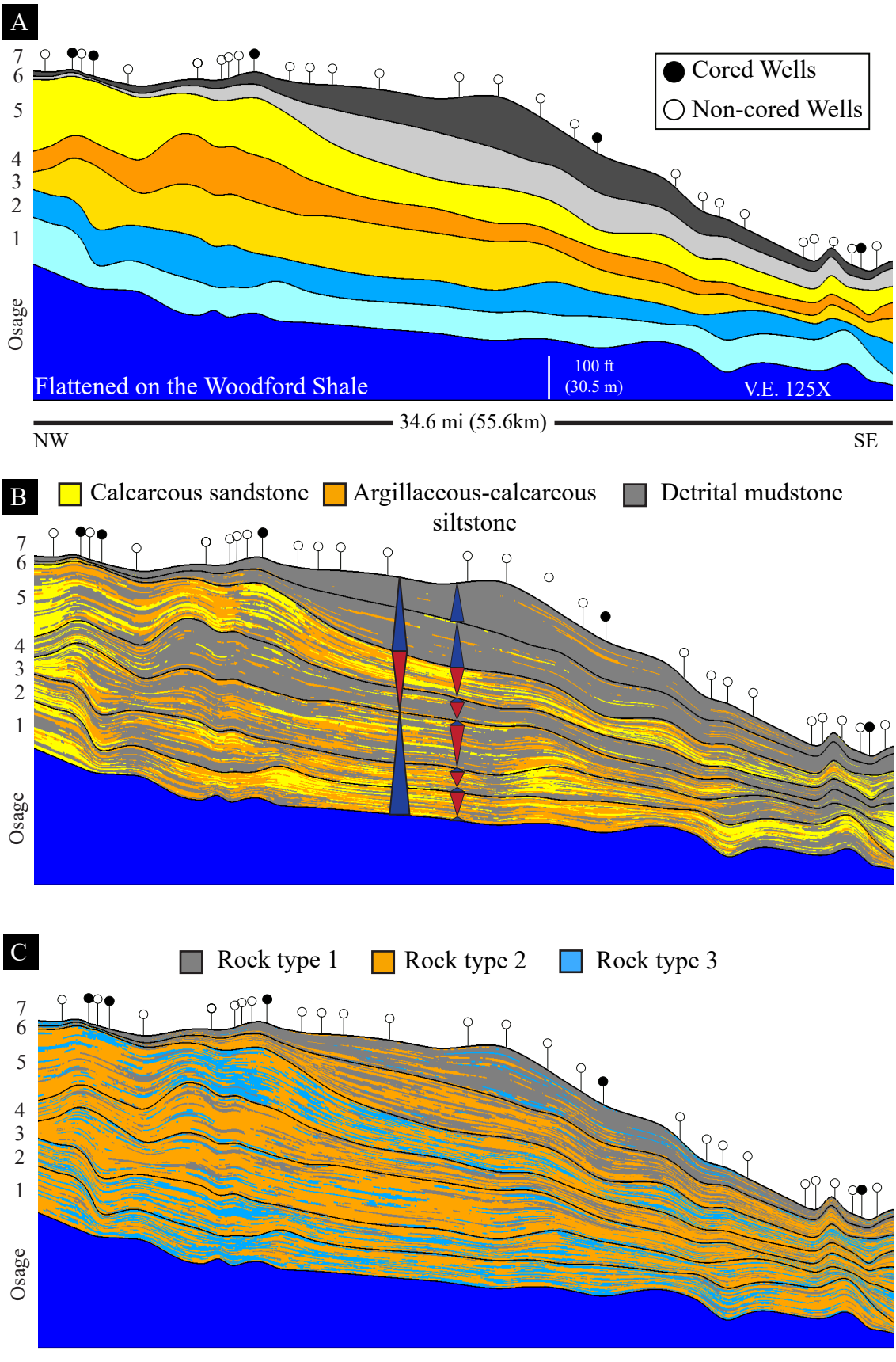
A
7
6
5
4
3
2
1
Osage
Cored Wells
Non-cored Wells
Flattened on the Woodford Shale
100 ft
(30.5 m)
V.E. 125X
34.6 mi (55.6km)
NW
SE
B
Calcareous sandstone
Argillaceous-calcareous siltstone
Detrital mudstone
C
Rock type 1
Rock type 2
Rock type 3

Figure 13: A) is a zone index model showing the stratigraphic zones through which chemofacies, rock types, water saturation, and effective porosity are modeled within. Zones are defined by the parasequences of the Meramec 1, 2, 3, 4, 5, 6 and 7 that were picked using Gamma Ray and the chemostratigraphic profiles of Ti and Zr. The models are flattened on the Woodford Shale top. Both cored and non-cored wells are displayed along the cross-section. B) the chemofacies model displays chemofacies distribution that exhibits a backstepping of calcareous rich chemofacies and an increasing of argillaceous rich chemofacies. from the Meramec 1 to 3 indicative of a transgressive sea level. As the chemofacies distribution in the Meramec 4 displays a similar level to slightly larger abundance of the detrital mudstone facies, it is interpreted to be a zone of aggredation. The Meramec 5 displays an abundance of calcareous rich facies indicating a regressive sea level. The Meramec 5 is topped by the very mudstone rich intervals of the Meramec 6 and 7 indicating a transgressive sea level. C) the rock type model exhibits a similar trend of rock type distributions from the Meramec 1 to the Meramec 4 rock type 3, the rock type most associated with calcareous facies, decreases. Rock type 2 which is associated with siliceous and argillaceous facies increases as well from Meramec 1 to 4, as rock type 1 associated with argillaceous facies indicating an increasing trend of porosity and decreasing trend of young's modulus. The Meramec 5 is abundant in rock type 3 indicating low porosity and high young's modulus. Meramec 6 and 7 is dominated by rock type 1 indicating high porosity and low Young's modulus.

%), which is interpreted to be a relatively deeper water environment. There is also a significant decrease in the calcareous sandstone chemofacies (25 % to 12 %), associated with a heavily cemented, calcareous and quartz-rich lithology. The argillaceous-calcareous siltstone, a transitional chemofacies that is also highly cemented and calcareous with slightly more clay than the calcareous sandstone, also decreases in abundance (40 % to 29 %) from Meramec 1 to 3. The top of the Meramec 3 is interpreted to be a maximum flooding surface and the Meramec 4 is interpreted to represent a period of aggradation as it maintains a similar chemofacies distribution proximally. Distally, the Meramec 4 appears to maintain a transgressive character, consisting of less argillaceous-calcareous siltstone (5 %) and calcareous sandstone (10 %) while the detrital mudstone chemofacies (85 %) dominates the distal portion of the Meramec 4 at a greater abundance than the Meramec 3. The proximal to distal variations of chemofacies in the Meramec 4 indicate an onset, or sharp transition from a retrogradational shoreline to aggradational, where proximally this aggradation is observed while distally, the chemofacies characteristic of aggradation is not exhibited. The study area for the chemofacies model is a more distal area of the Meramec ramp (compared to Miller, 2019) which explains the lower concentration of the calcareous sandstone and argillaceous-calcareous siltstone in parasequence 4 to the southeast of the study area. Meramec 5 interval appears to represent a progradational period as there is an abundance of the calcareous sandstone (30 %) and argillaceous-calcareous siltstone facies (33 %), and the zone has less detrital mudstone (37 %), indicating highly cemented and calcareous lithologies (detrital mudstone is the most abundant chemofacies at 60 % of the whole model, so despite it being numerically higher than the calcareous sandstone and argillaceous-calcareous siltstone, Meramec 5 has relatively low detrital mudstone). Meramec 6 and 7 transition back to a

retrogradational phase and are composed nearly exclusively of the detrital mudstone chemofacies (37 % to 97 %).

Spatial distribution of rock types

Rock types were modeled along the dip-oriented cross-section using sequential-indicator simulation (SIS). Model constraints included 1) chemofacies model, 2) upscaled rock type logs, 3) rock type percentages per zone, and 4) variogram parameters per rock type per zone.

The Meramec is composed of 3 rocks types that are modeled throughout the study area. Rock type 1 is a porous rock (5.8 vol%) displaying moderate water saturation (33 %) and low young's modulus (41 GPa), has the highest clay volume (27 wt %) and is associated with the detrital mudstone chemofacies. Rock type 2 has slightly less clay volume (24 wt %) than rock type 1 and is the most abundant rock type within the Meramec. Rock type 2 is highly associated with both the detrital mudstone and the argillaceous-calcareous siltstone chemofacies. This rock type has slightly less porosity (4.2 vol%) than rock type 1. Rock type 2 has the lowest water saturation (24 %) and a young's modulus between rock type 1 and 3. Rock type 3 is the highest in calcite volume (38 wt%) and lowest clay volume (14 wt%) with a resulting low porosity (2.3 vol %). This rock type is highly associated with the calcareous sandstone chemofacies. High water saturation (53 %) and young's modulus (53 GPa) is associated with rock type 3.

Rock type 2 is most abundant in the study area (68 %). Meramec 1, 2, 3 and 4 display an overall decrease of rock type 3 moving up section (35 % to 6 %), and an increase of rock types 1 (6 % to 23 %) and 2 (59 % to 71 %). This is indicative of increasingly optimal reservoir characteristics such as porous rocks (5 % to 7 %) with less water saturation (24 % to 22 %). Meramec 4 to Meramec 5 shows a rapid increase of rock type 3 (6 % to 31 %) suggestive of a

decrease in porosity (7 % to 5 %) and higher water saturation (22 % to 31 %). The decrease in porosity from Meramec 4 to 5 is rapid, displaying the same numeric porosity variation from the Meramec 1 to 4, which exhibited a more gradual increase over a thicker interval of deposition (even more variation from Meramec 4 to 5 for water saturation). Moving up section to the Meramec 6 and 7, rock types 2 (61 % to 13 %) and 3 (31 % to 7 %) decrease significantly and rock type 1 becomes the most abundant rock type (8 % to 81 %), indicating a very high porosity (14 %) but also very high water saturation (33 %). Although rock type 1 is generally associated with low water saturation, petrophysical property models show high water saturation (33 %) within the Meramec 6 and 7 with abundant clay and low permeability.

Spatial distributions of petrophysical properties

Effective porosity, water saturation and reservoir-quality indicator were modeled using sequential-Gaussian simulation (SGS) and were constrained by 1) chemofacies model, 2) upscaled porosity, water saturation and reservoir quality logs, 3) property histograms, and 4) variogram parameters by zone.

Figure 14 shows the stratigraphic variation of petrophysical property distribution within the Meramec. Meramec 1, 2, 3 and 4 show an overall increasing trend of effective porosity (5 % to 7 %) and decreasing water saturation (24 % to 22 %). Meramec E displays low porosity (5 %) and a sharp increase in water saturation (31 %) that continues through the Meramec 6 and 7 (33 %). Effective porosity distribution within the Meramec 6 and 7 exhibits an increasing porosity (5% to 14 %), indicating an association of high effective porosity and the detrital mudstone chemofacies. The reservoir quality indicator shows a laterally discontinuous distribution with no overall stratigraphic trend.

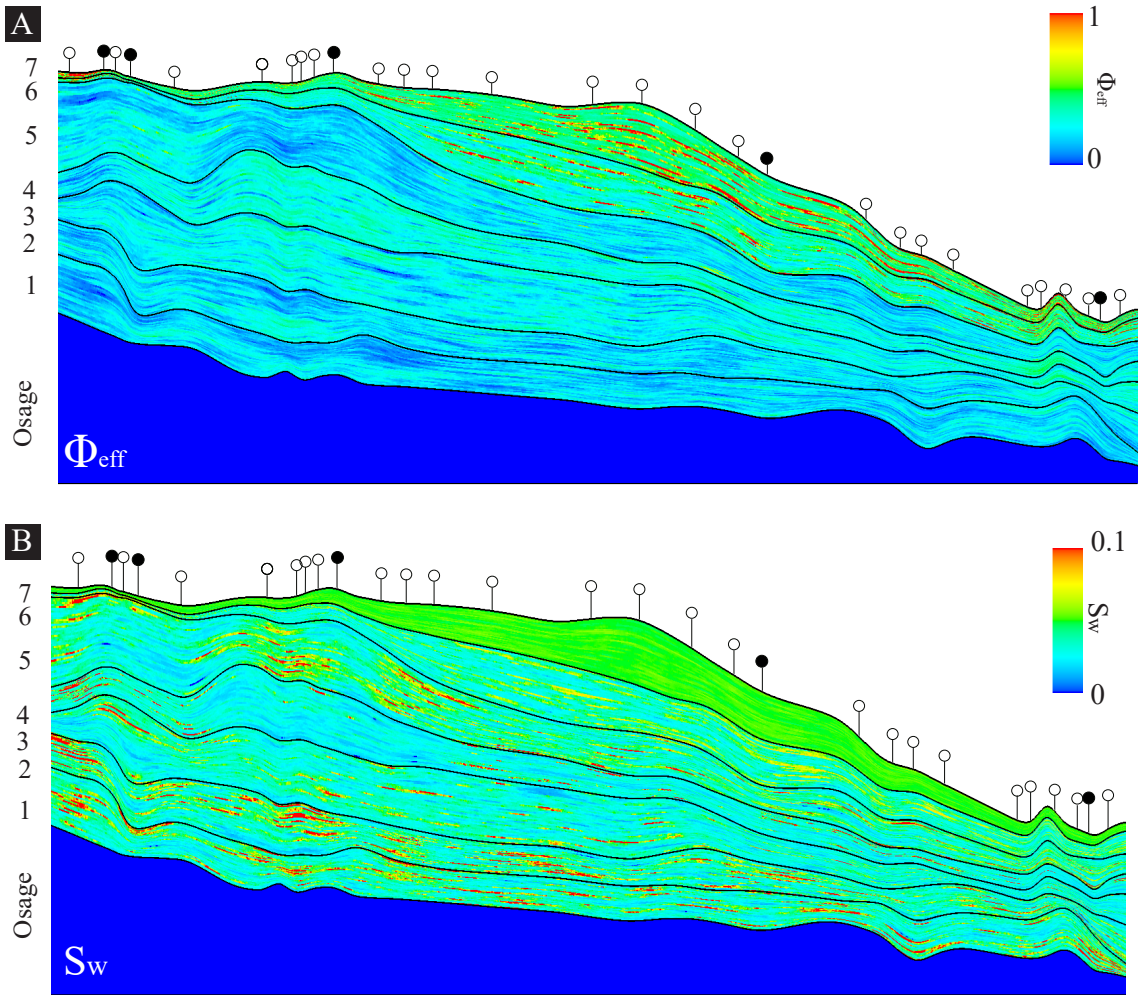

Figure 14: A) shows the effective porosity model of the Meramec. Meramec 1, 2, 3 and 4 exhibits an overall increasing trend of effective porosity. Porosity decreases in the Meramec 5 and then increases towards the top of the Meramec in zones 6 and 7. B) shows the water saturation model of the Meramec. Parasequences 1, 2, 3 and 4 exhibits an overall decreasing trend of water saturation. Water saturation increases in the Meramec 5. The Meramec parasequences 6 and 7 show laterally extensive moderate to high water saturation throughout.

Production analysis

Chemofacies distribution, rock type distribution, average effective porosity, and average water saturation along the lateral of 5 producing horizontal wells was compared to 60-, 90- and 120-day cumulative oil production data. Figure 15 shows the relationships between oil production and reservoir properties. A strong positive correlation (83 %) between prolific wells and high percentages of the detrital mudstone chemofacies along the lateral is observed. The argillaceous-calcareous chemofacies shows a negative correlation (-67 %) with the higher producing wells and the calcareous sandstone chemofacies displays a strong negative correlation (-83 %) to well production. Rock type distrubtion along the laterals show little correlation to oil production (Appendix-F1). Average effective porosity has a positive correlation (72%) to the 60-, 90- and 120-day cumulative oil production whereas reservoir quality indicator has some correlation (69 %). Water saturation has a weaker positive correlation (25 %) to oil production. Production drivers from this study include an abundance of detrital mudstone chemofacies and effective porosity.

DISCUSSION

Depositional controls on production drivers

Based on oil production data and chemofacies from 5 wells, the detrital mudstone chemofacies appears to be a driver of oil production. The detrital mudstone chemofacies is associated with high concentrations of Ti and Zr, continentally-derived proxies, and Al and K, clay-sourced proxies. Proximally, the detrital mudstone has moderate concentrations of Si/Al and Si/Ti, proxies for quartz, this facies becomes slightly more concentrated in these quartz proxies basinwards. The detrital mudstone is associated with low concentrations of Ca and Sr, proxies for carbonate sourced grains or cement. The detrital mudstone is also associated with high

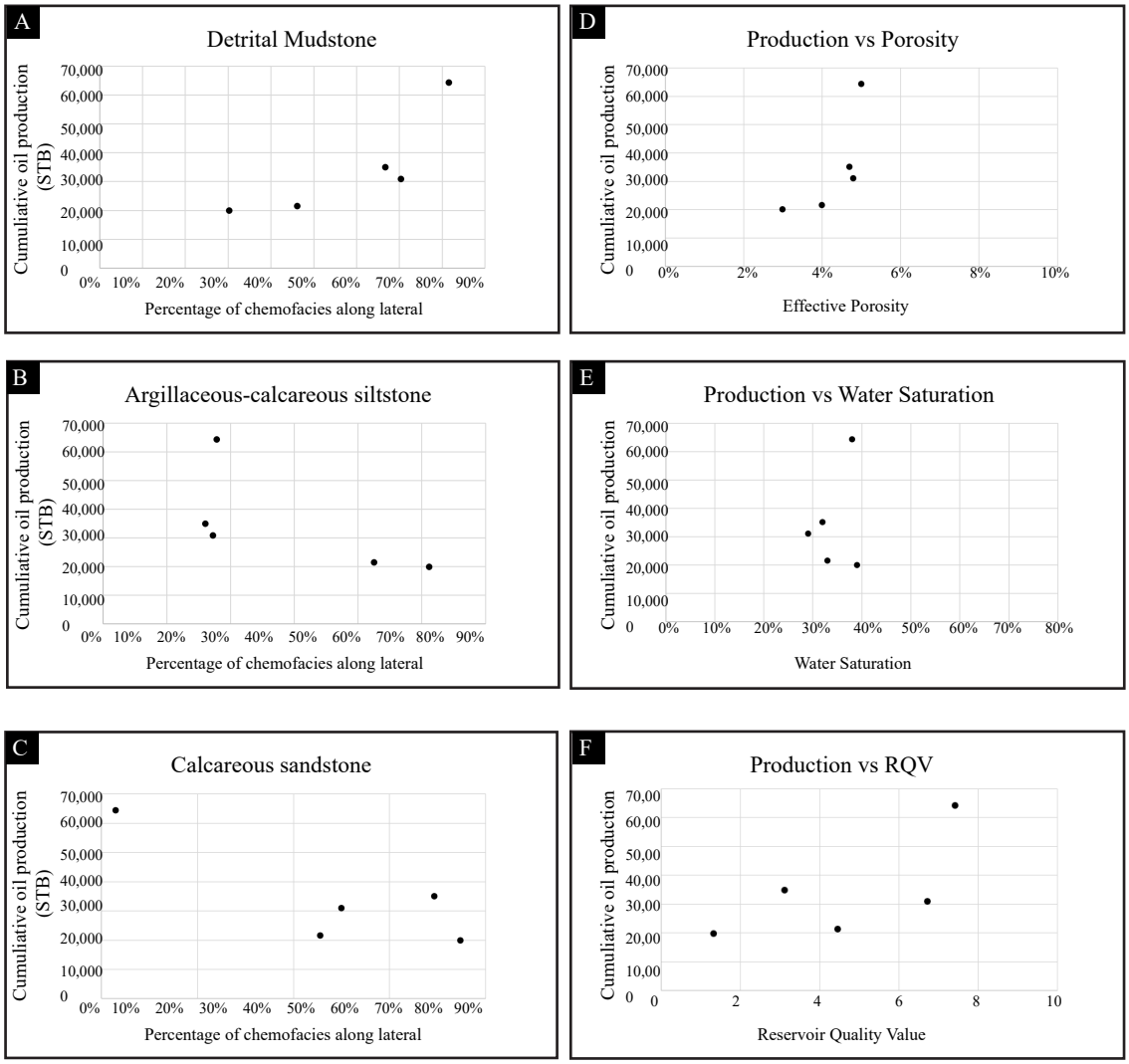

Figure 15: Cumulative oil production for 120-days are compared to percentage of chemofacies, effective porosity, water saturation and reservoir quality along the lateral for five producing wells. A strong positive correlation between detrital mudstone and production is shown, while argillaceous-calcareous siltstone and calcareous sandstones show a strong negative correlation with production. Porosity and reservoir quality show a positive correlation where water saturation shows little correlation to cumulative oil production.

concentrations of Sr/Ca indicative of minor diagenetic cementation. The predominate control on chemofacies can be tied directly to its carbonate, clay and continentally-derived proxies. Basinward, quartz proxy concentrations increase within the detrital mudstone chemofacies. The mudstone in this sense is not a true shale, rather, sufficient quartz grains are present within the facies and the clay within the matrix prevents calcite cementation and preserves porosity rather than a true shale, where clay-filled matrices diminishes porosity. Despite the argillaceous nature of this chemofacies, quartz grains are present in sufficient abundance to maintain high effective porosity, which is also highly correlative (83 %) to high cumulative oil production.

The argillaceous-calcareous siltstone chemofacies is denoted by moderate concentrations of each indicator element with high diagenetic alteration as implied by the low Sr/Ca level observed in this chemofacies. The argillaceous-calcareous siltstone is a mixed detrital-sourced silt and carbonate-sourced rock that is highly cemented. The quartz in this chemofacies is highly associated with continentally sourced proxies, indicating the cement is mostly due to carbonate diagenesis rather than quartz overgrowth. This mixed chemofacies has a strong negative correlation to oil production, likely due to its abundance in calcite cement and associated low porosity.

The calcareous sandstone chemofacies show a negative correlation to production (-83 %). It is characterized by very high carbonate and quartz proxies and is a moderately cemented due to carbonate diagenesis. This chemofacies has Si/Al and Si/Ti that sometimes crossover with Zr, indicating a mixed detrital and biogenic-sourced quartz. Biogenic sourced-quartz is inclined to overgrowth when there is not clay present to coat the quartz grains. The cement in the calcareous sandstone chemofacies is likely due to both diagenetic calcite cementation and quartz overgrowth, as clay proxies are minimal indicating the quartz grains are not coated to prevent

such overgrowths. This highly cemented sandstone is associated with low effective porosity, and low oil production for the Meramec. The calcareous sandstone chemofacies likely shows little correlation to production due to it being the least abundant chemofacies and limited sample size.

Stratigraphic controls on reservoir quality

Parasequences with an abundance of both detrital mudstone chemofacies and rock types 1 and 2 in the Meramec are associated with high reservoir quality. Meramec parasequences 3 and 4 are comprised predominately of detrital mudstone and rock types 1 and 2, which corresponds to higher effective porosity (6.5 % to 7.4 %) and low water saturation (0.24 % to 0.22 %). These parasequences with high reservoir quality border the maximum flooding surface and represent the turning point of a transgressive sea level to a regressive environment. The stratigraphic distribution of this combination of detrital mudstone (60 % to 84 %) and rock type 2 (71 % to 74 %) corresponds to overall transgressive sea level and also exists at the base of each shallowing-upward parasequence. In the Meramec 6 and 7, detrital mudstone is abundant (91 % to 97 %), and rock type 1 dominates (80 %) but these parasequences are highly saturated with water (33 %), resulting in the swelling of clays and likely depleating permeability. Due to the association of these parasequences with high water saturation, the reservoir quality is low in comparison to the detrital mudstone rich parasequences 3 and 4. Parasequences that correspond to regressive environment such as the Meramec 5 are associated with high levels of calcareous sandstone chemofacies (30%), the chemofacies highly associated with mixed biogenic and detrital-sourced quartz. Biogenic quartz is harder than detrital and has been associated with bit trips during drilling. Because biogenic quartz can only be interpreted confidintely within the calcareous sandstone chemofacies, zones with high levels of the calcareous sandstone chemofacies be predicted with triple combo well logs and avoided during drilling to prevent bit trips.

CONCLUSIONS

The Meramec series in the STACK Play of central Oklahoma is made up of mixed carbonate and siliceous sediments that were deposited on a regionally extensive shelf in relatively shallow water with highly frequent sea level cycles. Sea level cyclicity resulted in the complex stacking patterns and lateral distribution of facies and chemofacies within the Mississippian. The Meramec is comprised of 3 chemofacies including detrital mudstone, argillaceous-calcareous siltstone and calcareous sandstone. Related to the chemofacies, the Meramec is also comprised of 3 rock types based on the relationships of core-derived porosity and permeability measurements using the flow-zone indicator (FZI) methodology for rock type classification. Random Forest, a supervised machine learning technique, achieved up to 83% overall accuracy for predicting chemofacies. The log suite input for Random Forest used to train and predict chemofacies include GR, RHOB, and NPHI.

The Mississippian Meramec consists of 7 shallowing upward parasequences that display stacking patterns of chemofacies indicating a transgressive-regressive-transgressive succession. The stacking patterns of the chemofacies show an overall retrogradational trend overlain by an aggradational and a progradational parasequence. The chemofacies stacking pattern and rock type distributions are interpreted to be a control on the distribution of optimal reservoir quality parameters including effective porosity and water saturation.

When chemofacies and petrophysical properties are compared to cumulative oil production data, drivers of high productivity include an abundance of detrital mudstone chemofacies, rock type 1, and high effective porosity. Detrital mudstone is interpreted to be composed of continentally-sourced silts, clay and quartz where there is sufficient clay to coat quartz grains and fill the matrix such that quartz and calcite cementation is prevented and

primary porosity is preserved. Argillaceous-calcareous siltstones and calcareous sandstones are associated with higher cementation resulting in the depletion of porosity. The argillaceous-calcareous siltstone cement appears to be dominated by diagenetic cementation whereas the calcareous sandstone is interpreted to have a mixed source of cementation. The calcareous sandstone contains more biogenic quartz and a resulting higher brittleness and intervals with high concentrations of this chemofacies can be flagged as intervals that may require more frequent bit trips. The argillaceous-calcareous siltstone and calcareous sandstone chemofacies are correlated to low productivity. The Meramec parasequences 3 and 4 consist of higher distributions of detrital mudstone and rock types 1 and 2 and exhibit higher porosity and lower water saturation, indicating these parasequences have the combination of depositional characteristics and petrophysical properties that yield ideal reservoir quality.

REFERENCES

Adler, F.J., et.al, 1987, Basement Structure of the Mid-Continent: American Association of Petroleum Geologists Memoir, v. 15, p.1000–1004.

Ball, M. M., M. E. Henry, and S. E. Frezon, 1991, Petroleum geology of the Anadarko Basin Region, Province (115), Kansas, Oklahoma, and Texas: Department of the Interior U.S. Geological Survey, 36 p.

Banner, J.L. 1995. Application of the trace element and isotope geochemistry of strontium to studies of carbonate diagenesis: Sedimentology, v. 42, p. 805–824.

Beebe, B.W., 1959, Characteristics of Mississippian Production in the Northwestern Anadarko Basin: Tulsa Geological Society Digest, v. 27, p. 190–205.

Birch, C. B., 2015, Reservoir-scale stratigraphy, sedimentology and porosity characteristics of Mississippian reservoirs, northeastern Anadarko shelf, Oklahoma, M.S. Thesis, University of Oklahoma, Norman, Oklahoma, 90 p.

Blakey, R., 2011, Paleogeography and geologic evolution of North America, http://cpgeosystems.com/paleomaps.html, (accessed March 2018).

Boyd, D.T., 2008, Stratigraphic guide to Oklahoma oil and gas reservoirs: Oklahoma Geological Society, Special Publication 2008-1, 2p.

Burmsack, H.J., 2006. The trace metal content of recent organic carbon-rich sediments: Implications for Cretaceous black shale formation. Paleogeography, Paleoclimatology, Palaeoecology, v.232, p. 344–361

Campbell, J. A., C. J. Mankin, A. B. Schwarzkopf, and J. J. Raymer, 1988, Habitat of petroleum in Permian rocks of the midcontinent region; in, Permian Rock of the Midcontinent, W. A. Morgan and J. A. Babcock, eds.: Midcontinent Society of Economic Paleontologists and Mineralogists, Special Publication No. 1, p. 13–35.

Curtis, D.M., and Champlin, S.C., 1959, Depositional Environments of Mississippian Limestones of Oklahoma, Tulsa Geological Society Digest, V. 27, No. 1, p. 90–103.

Drummond, K., 2018, Regional stratigraphy and proximal to distal variation of lithology and porosity within a mixed carbonate-siliciclastic system, Meramec and Osage series (Mississippian), central Oklahoma, M.S. Thesis, University of Oklahoma, Norman, Oklahoma, 165 p.

Duarte, D., 2018, Rock characterization and stratigraphy of the Mississippian strata, Meramec/Sycamore merge play, central Oklahoma, M.S. Thesis, University of Oklahoma, Norman Oklahoma, 80 p.

Dutton, S.P., 1984, Fan-Delta Granite Wash of the Texas panhandle, Oklahoma City Geological Society, vol. Short Course Notes.

Flinton, K. C., 2016, The effects of high-frequency cyclicity on reservoir characteristics of the "Mississippian limestone", Anadarko Basin, Kingfisher County, Oklahoma: Master's thesis, Oklahoma State University, Stillwater, OK, 412 p.

Given, R.K. and B.H. Wilkinson, 1985, Kinetic control of morphology, composition and mineralogy of abiotic sedimentarty carbonates: Journal of Sedimentary Petrology, v. 55, p.109–119

Grammer G. M., D. Boardman, J. Puckette, J. Gregg, J. Priyank., M. Childress, B.J. Price, B. Vanden Berg, and S. LeBlanc, 2013, Integrated reservoir characterization of Mississippian-age Midcontinent carbonates: AAPG Search and Discovery Article #30297, 31 p.

Han, Heyleem et al., 2019, X-ray Fluorescence and laser induced breakdown spectroscopy for advanced rock elemental analysis: Unconventional Resources Technology Conference (URTEC), Article #1072

Haq, B. U., and Schutter, 2008, A chronology of Paleozoic sea-level changes: Science, v. 322, p.64–68.

Hardwick, J., 2018, Reservoir quality evaluation of the Meramec and Upper Osage units in the Anadarko Basin, M.S. Thesis, University of Oklahoma, Norman, Oklahoma, 76 p.

Hickman, G., 2018, Parasequence-scale stratigraphic variability of lithology and porosity of Mississippian Meramec reservoirs and the relationships to production characteristics, STACK trend, Oklahoma, M.S. Thesis, University of Oklahoma, Norman, Oklahoma, 150p.

Kumar, B. and M. Kishore, 2006, Electrofacies classification - a critical approach: 6th International conference and exposition on petroleum geophysics, Kilkata, India, p. 822–825.

Lane, H.R., and T.L. De Keyser, 1980, Paleogeography of the Late Early Mississippian (Tournaisian 3) in the Central and Southwestern United States: SEPM, Rocky Mountain Symposium 1, p. 149–162.

Leavitt, A., 2018, Depositional systems of the STACK and SCOOP Mississippian units; regional understanding from logs and core, Oklahoma Geological Survey, STACK Play Workshop Technical Program & Core Viewing, Oklahoma City, Oklahoma.

LeBlanc, S.E., 2014, High resolution sequence stratigraphy and reservoir characterization of the "Mississippi Limestone" in north-central Oklahoma, M.S. Thesis, Oklahoma State University, Stillwater, Oklahoma, 443 p.

Lindzey, K. M 2015, Geologically constrained seismic characterization and 3-D reservoir modeling of Mississippian reservoirs, north-central Anadarko shelf, Oklahoma: M.S. Thesis, University of Oklahoma, Norman, Oklahoma, 106 p.

Mazzullo, S.J., 2011, Mississippian oil reservoirs in the southern Midcontinent: new exploration concepts for a mature reservoir objective: Search and Discovery Article #10373.

Mazzullo, S.J., B.W. Wilhite, D.R. Boardman, B.T. Morris., and C.J. Godwin, 2016, Stratigraphic architecture and petroleum reservoirs in lower to middle Mississippian strata (Kinderhookian to basal Meramecian) in subsurface central to southern Kansas and northern Oklahoma: Shale Shaker, vol. 67 no. 2, p. 20–49.

McConnell, D.A., M.J. Goyda, G.N. Smith, and J.P. Chitwood, 1989, Morphology of the frontal fault zone, southwest Oklahoma: Implications for deformation and deposition on the Wichita Uplift and Anadarko Basin: Geology, vol. 18, no. 7, p. 34–637

Miller, J., 2018, Regional stratigraphy and organic richness of the Mississippian Meramec and associated strata, Anadarko Basin, central Oklahoma, M.S. Thesis, University of Oklahoma, Norman, Oklahoma, 154 p.

Miller, M., 2019, Mississippian Meramec lithologies and petrophysical property variability, STACK trend, Anadarko Basin, Oklahoma, M.S. Thesis, University of Oklahoma, Norman, Oklahoma, 60 p.

Northcutt, R.A., and J.A. Campell, 1995, Geologic provinces of Oklahoma: Oklahoma Geological Survey Open-File Report 5–95, 1 sheet, scale 1:750000, 6-page explanation and bibliography.

Northcutt, R.A., K.S. Johnson, and G.C. Hinshaw, 2001, Geology and petroleum reservoirs in Silurian, Devonian, and Mississippian rocks in Oklahoma: Oklahoma Geological Survey Circular 105, p. 1–15.

Parham, K.D., and R.A. Northcutt, 1993, Mississippian chert and carbonate and basal Pennsylvanian sandstone – central Kansas uplift and northern Oklahoma, D. Bebout, W. White, and T. Hentz, eds.: Atlas of major Midcontinent gas reservoirs, Austin, Bureau of Economic Geology, p. 57–59.

Pearce, T.J., B.M. Besly, D.S. Wray, and D.K. Wright, 1999. Chemostratigraphy: a method to improve interwell correlation in barren sequences- a case study using onshore Duckmantian/Stephanian sequences (West Midlands, U.K.): Sedimentary Geology, 124, p. 197–220.

Pearce, T.J. & Jarvis, I. 1992. Applications of geochemical data to modelling sediment dispersal patterns in distal turbidites: Late Quaternary of the Madeira Abyssal Plain: Journal of Sedimentary Petrology, 62, p. 1112-1129.

Peeler, J.A., 1985, Reservoir characterization of the Mississippian “chat,” Hardtner field, southern Barber County, Kansas, M.S. Thesis, Wichita State University, Wichita, Kansas, p. 120.

Perry, W.J., 1990, Tectonic evolution of the Anadarko Basin region, Oklahoma: Department of the Interior, U.S. Geological Survey, no. 1866 – A, 19 p.

Price, B., K. Haustveit, and A. Lamb, 2017, Influence of stratigraphy on barriers to fracture growth and completion optimization in the Meramec Stack Play, Anadarko Basin, Oklahoma: Unconventional Resources Technology Conference (URTEC), Article #2697585, 8 p.

Sageman, B.B., and T.W. Lyons, Geochemistry of fine-grained sediments and sedimentary rocks: Mackenzie, F. (ed.) Sediments, Diagenesis, and Sedimentary Rock Treatise on Geochemistry, v. 7, p. 115–158.

Trevino, Andrea, 2016, Introduction to K-means Clustering: Oracle + DataScience.com

Tribovillard, N., T.J. Algeo, T.W. Lyons, and A. Riboulleau, 2006, Trace metals as paleoredox and paleoproductivity proxies: An update: Chem. Geol., v. 232, p. 12–32.

Turner, B.W., 2016, Utilization of chemostratigraphic proxies for generating and refining sequence stratigraphic frameworks in mudrocks and shales, Dissertation, University of Oklahoma, Norman, Oklahoma, p. 32–35.

Tucker, M.E., 1981, Sedimentary Petrology, an Introduction: Oxford, Blackwell Scientific Publications, 252 p.

APPENDIX A: Geologic Setting

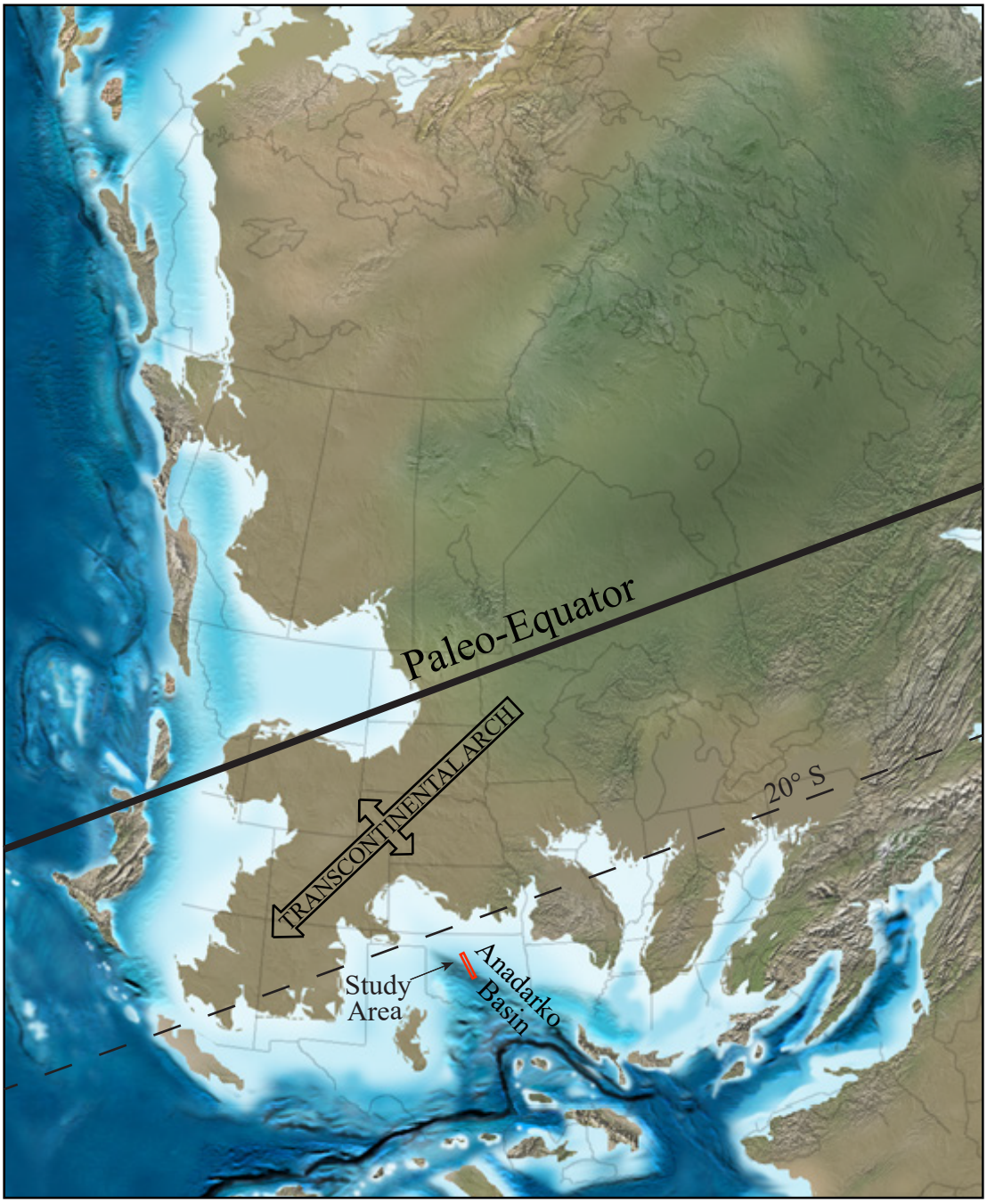

Appendix-A1: Late Mississippian paleogeographic map modified from (Blakey, 2011). The study area is outlined in red within the Anadarko basin at about 20° S of the paleoequator.

APPENDIX B: Core data

APPENDIX-B1: Well A core description

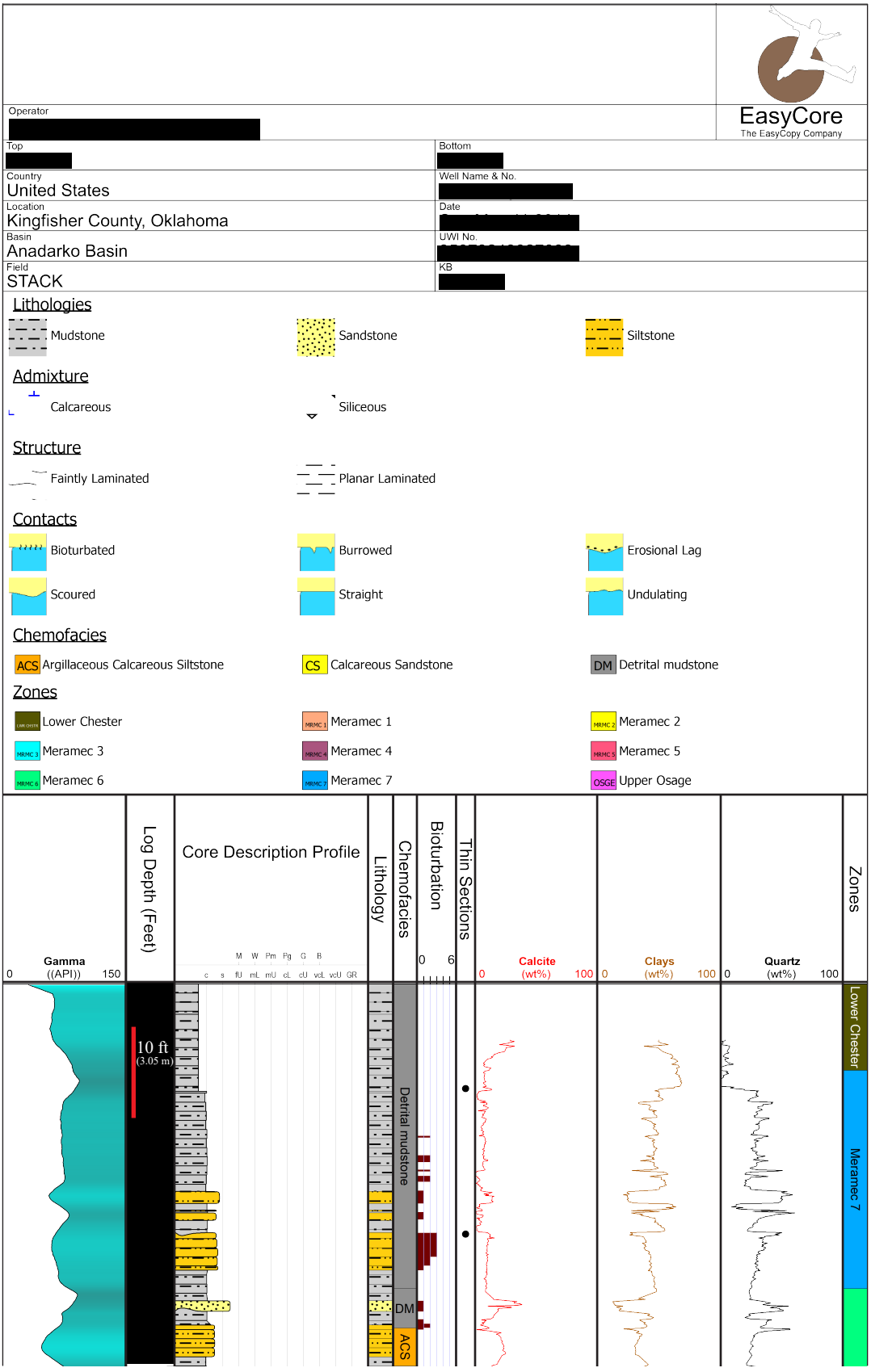

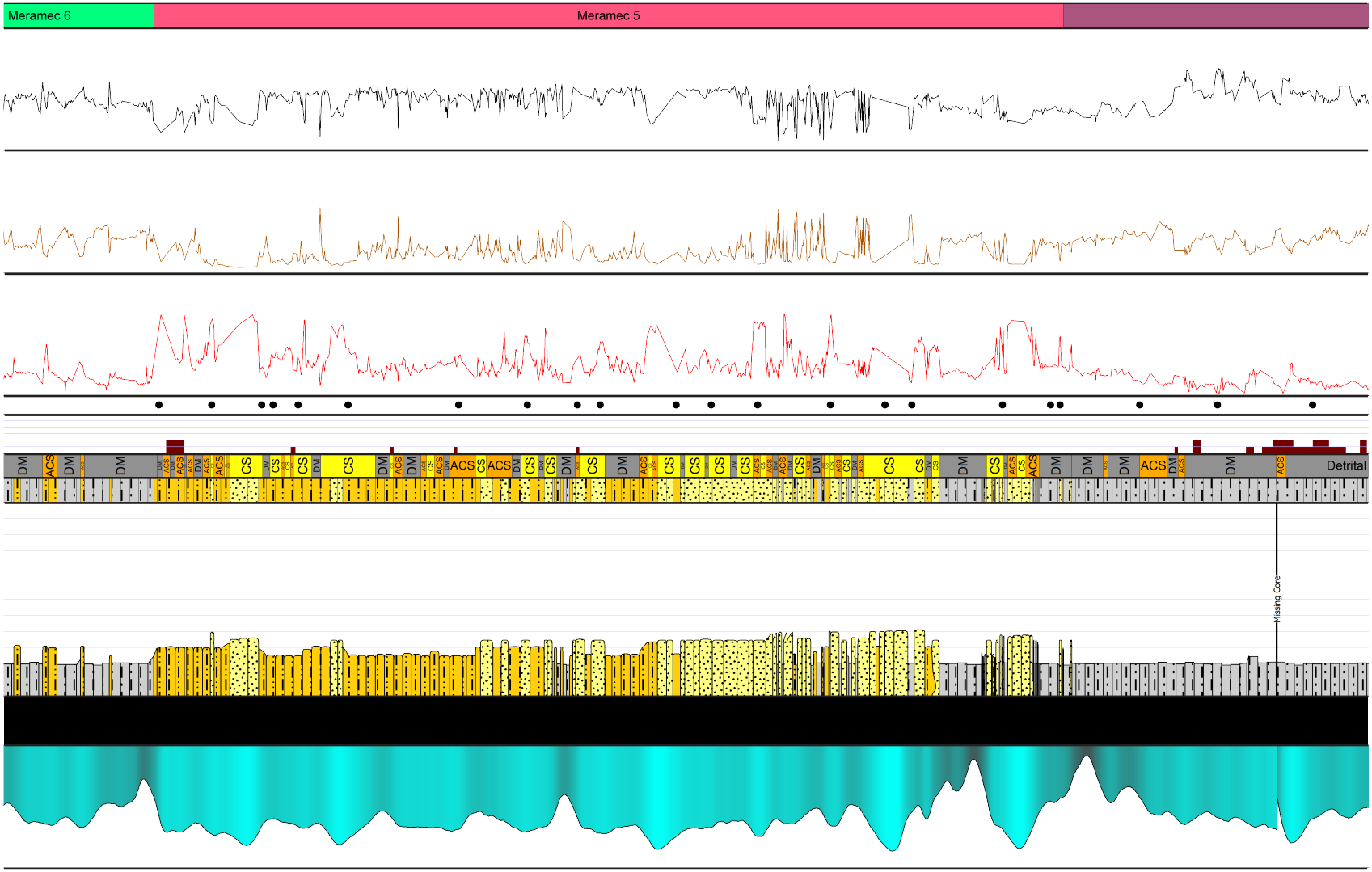
Meramec 6
Meramec 5
DM
ACS
CS
Detrital
Missing Core

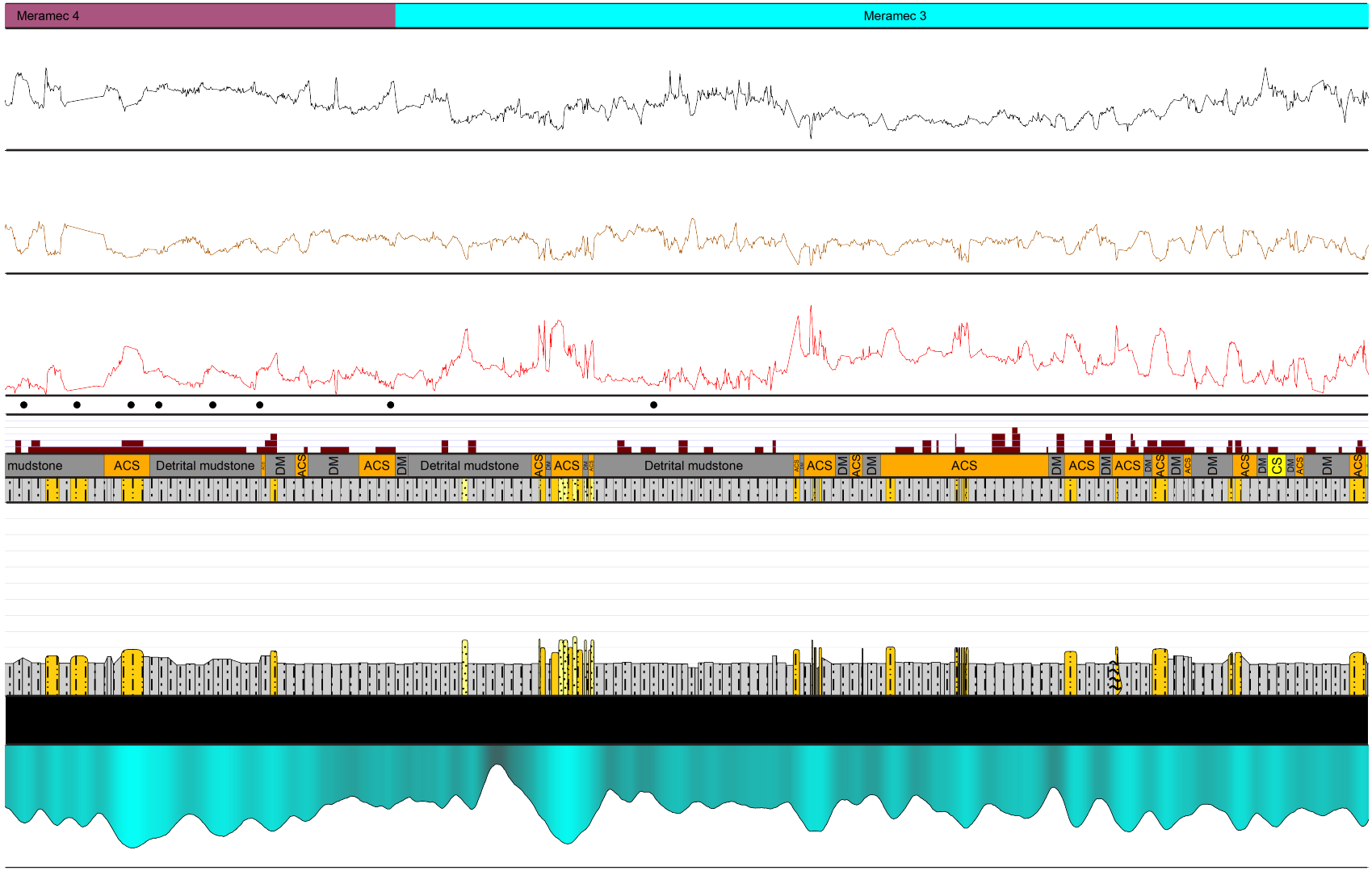
Meramec 4
Meramec 3
mudstone
ACS
Detrital mudstone
DM
ACS
DM
ACS
DM
Detrital mudstone
ACS
ACS
Detrital mudstone
ACS
ACS
DM
ACS
DM
ACS
DM
ACS
DM
ACS
DM
ACS
DM
ACS
DM
ACS
DM
CS
DM
ACS
DM
ACS

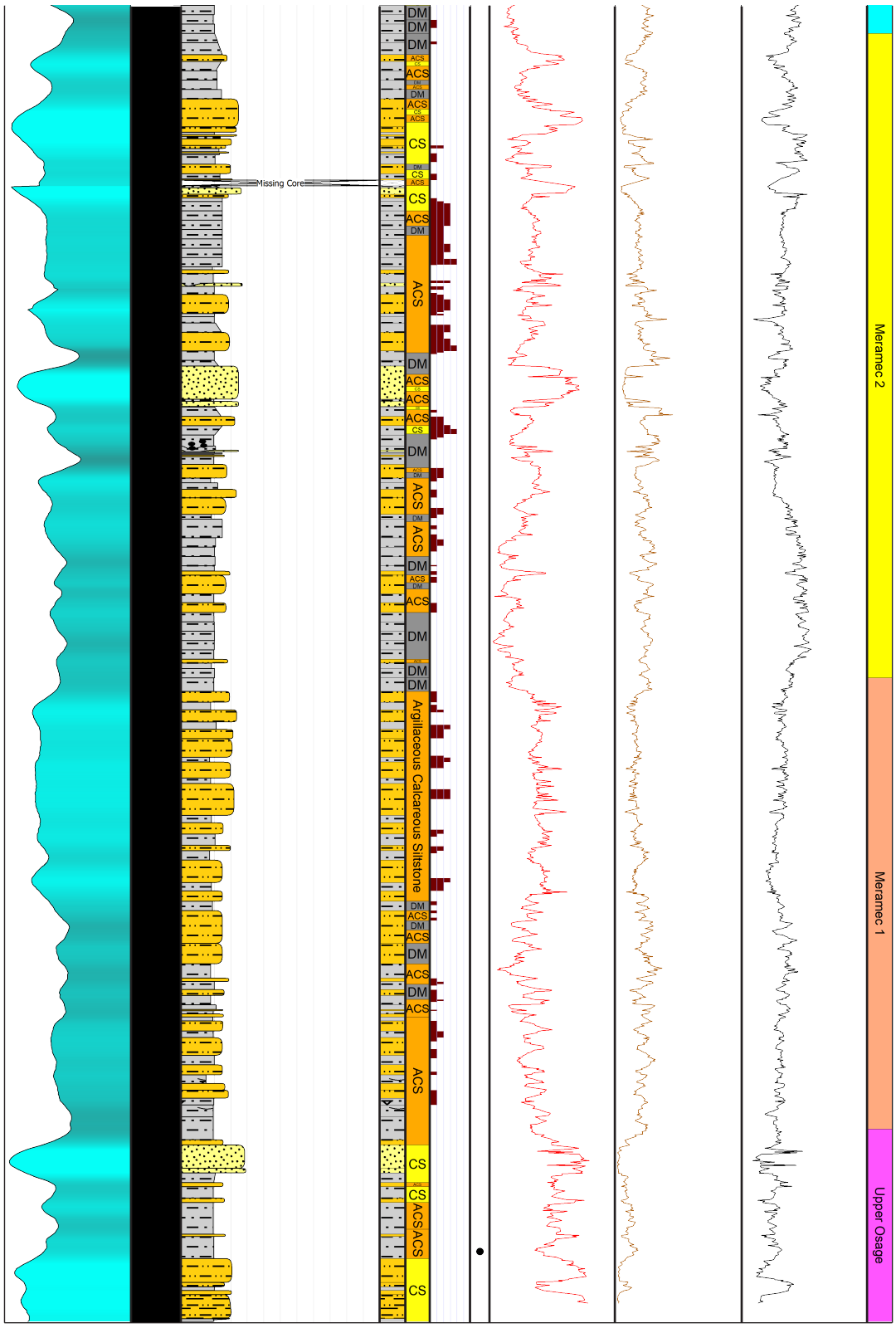
Meramec 2
Meramec 1
Upper Osage
Missing Core
Argillaceous Calcareous Siltstone
DM
ACS
CS

APPENDIX-B2: Well B core description

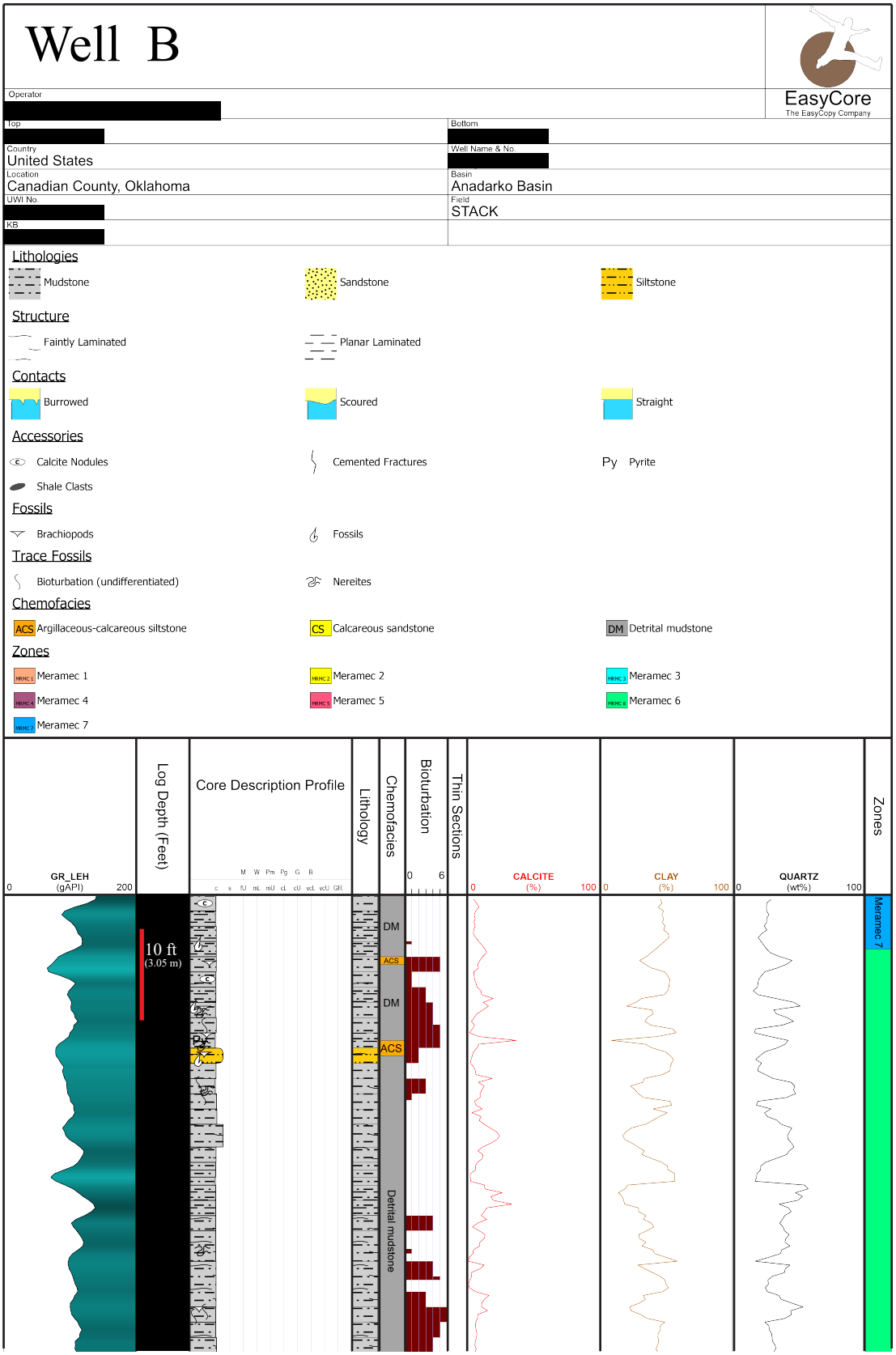

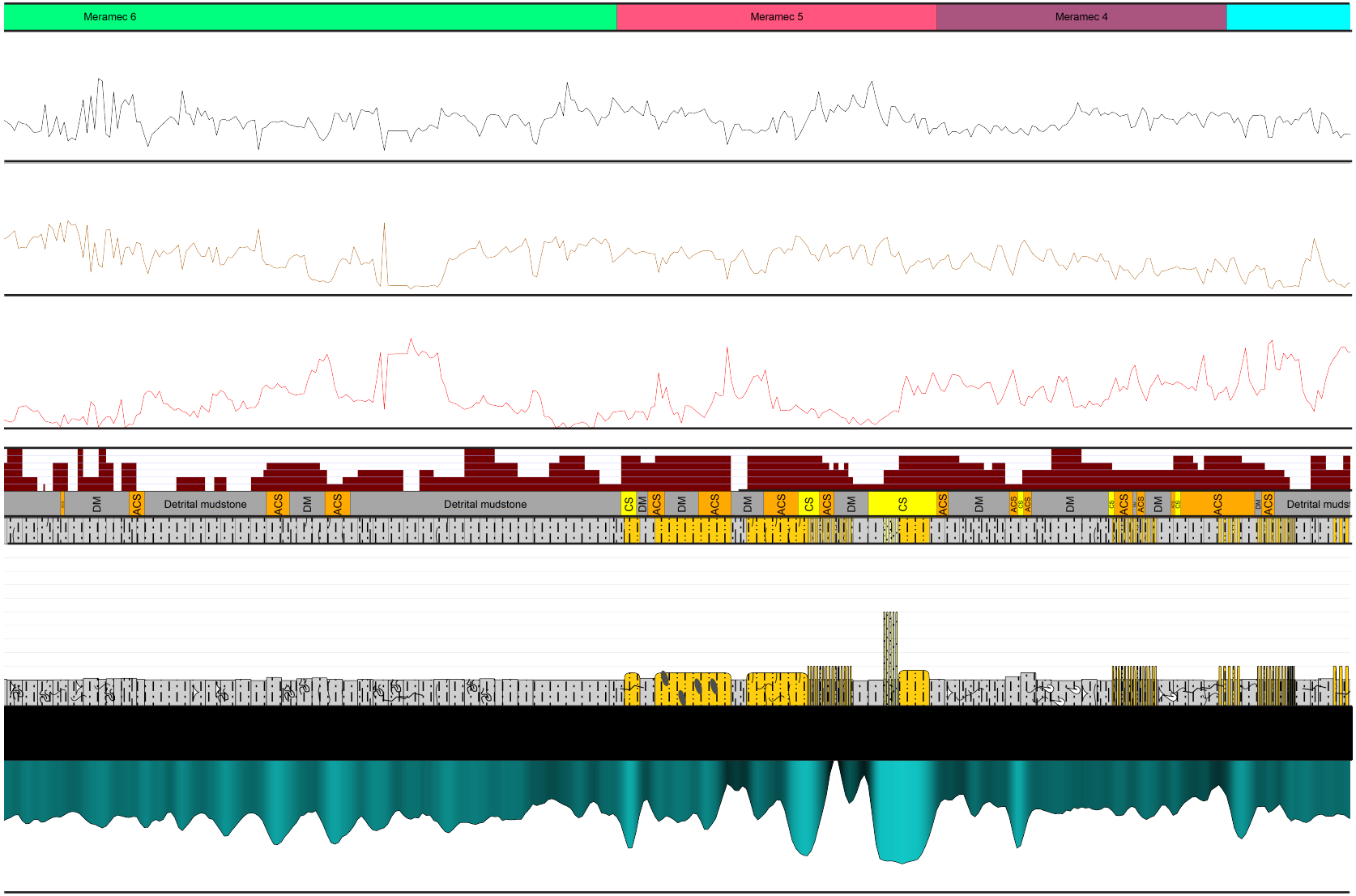
Meramec 6
Meramec 5
Meramec 4
DM
ACS
Detrital mudstone
CS

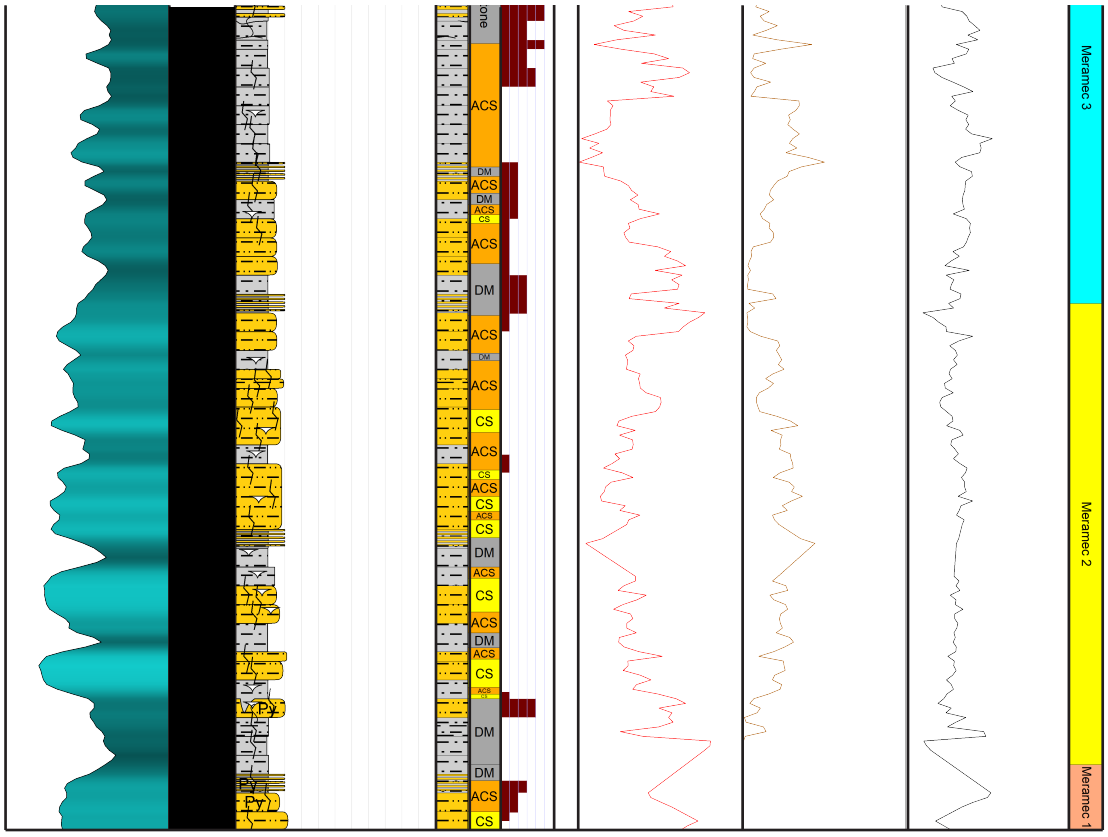
Meramec 3
Meramec 2
Meramec 1
one
ACS
DM
CS
Py

APPENDIX-B3: Well C core description

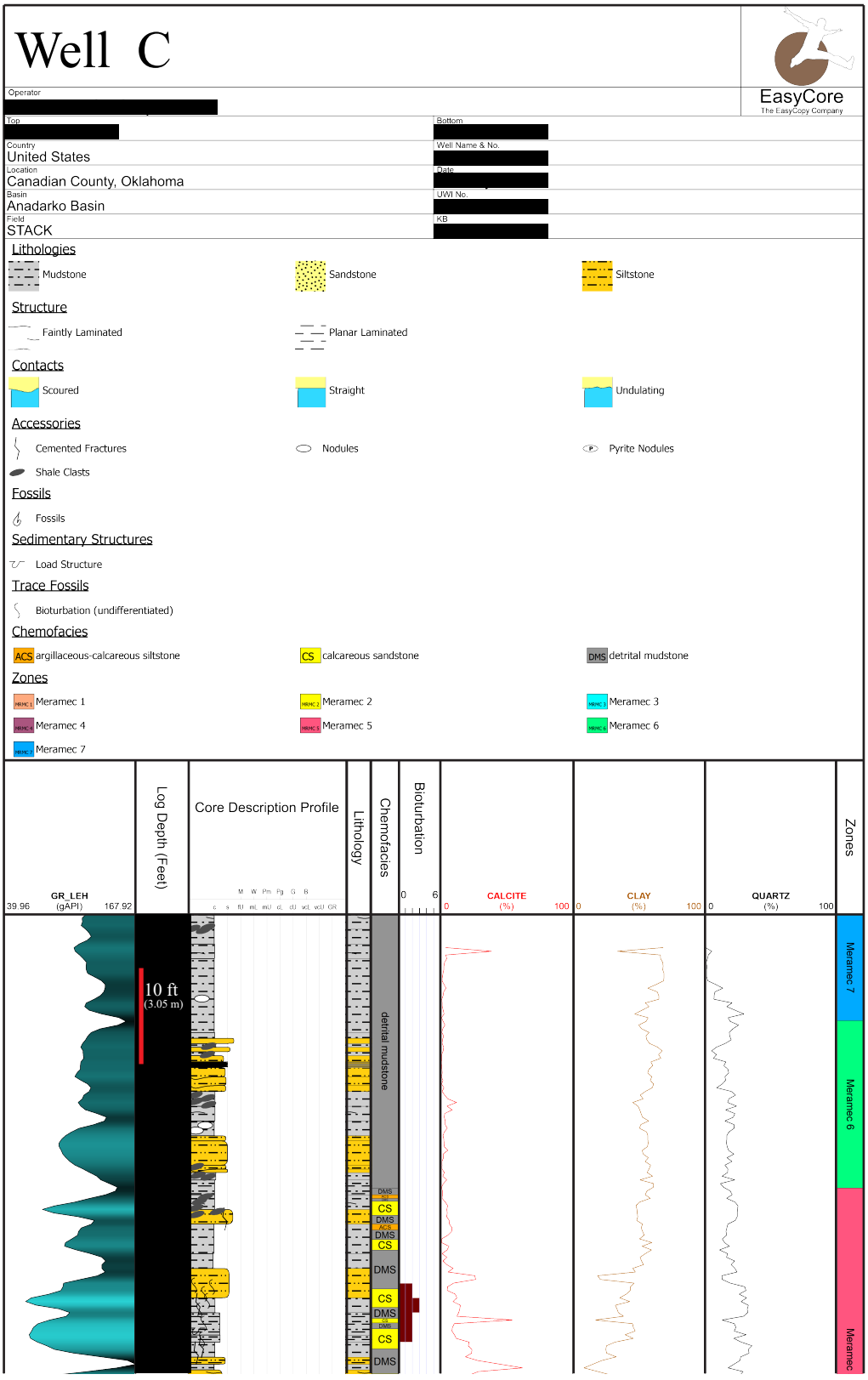

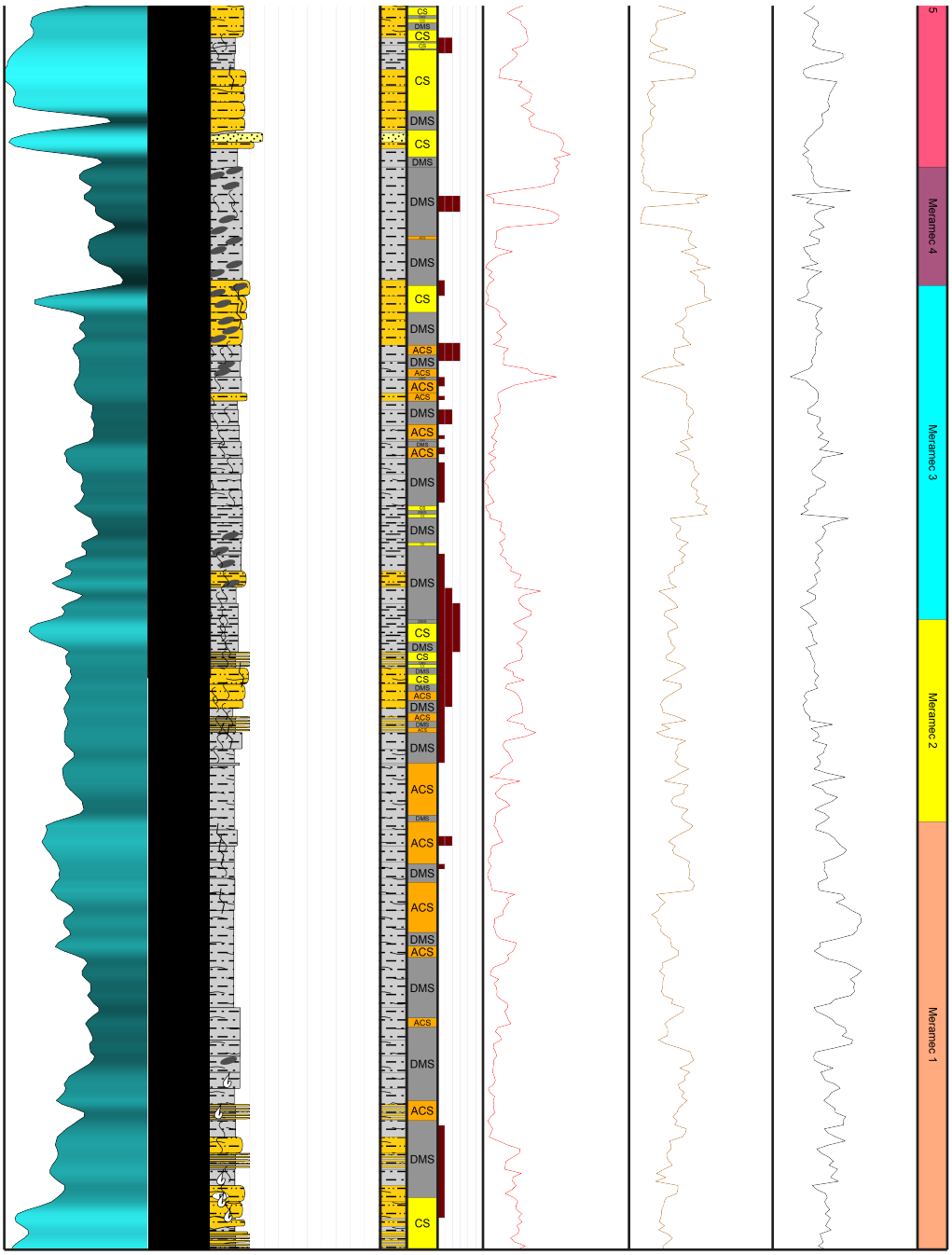
5
Meramec 4
Meramec 3
Meramec 2
Meramec 1
CS
DMS
ACS

APPENDIX C: Chemofacies and Indicator Element Definition

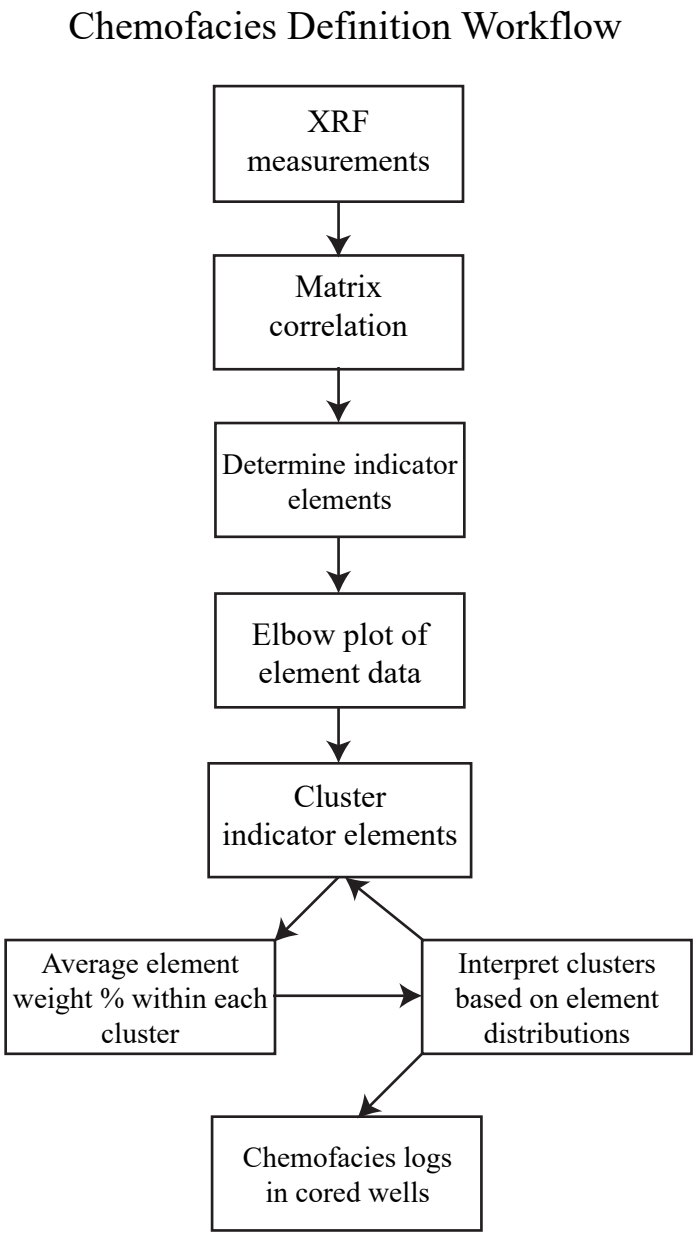

Appendix-C1: Defining chemofacies involves a detailed literature review and matrix correlation to determine which elements should be used as environmental proxies for clustering. Elbow plots can be used to identify the optimal number of clusters. However, testing multiple classifications with varying numbers of clusters is critical to ensure all facies that exist are represented.

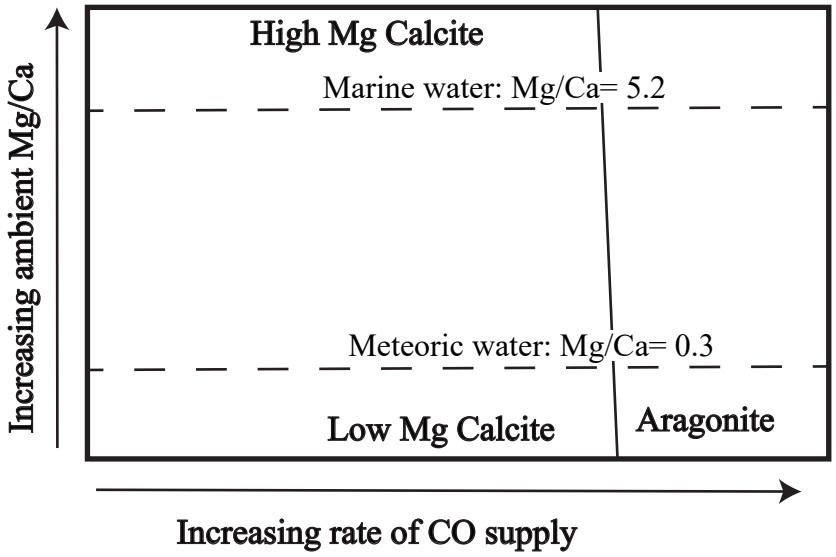

Appendix-C2: Cutoffs of Mg/Ca within calcite cement are used to determine environment of diagenesis. Diagenetic cementation within marine water have high levels of magnesium displayinig a Mg/Ca level of 5.2 or higher. In meteoric waters, the cement would far less Mg, with a level of 0.3 Mg/Ca or less. The cement within Well A had a Mg/Ca ratio of 0.13 indicating the diagenesis was metoric.

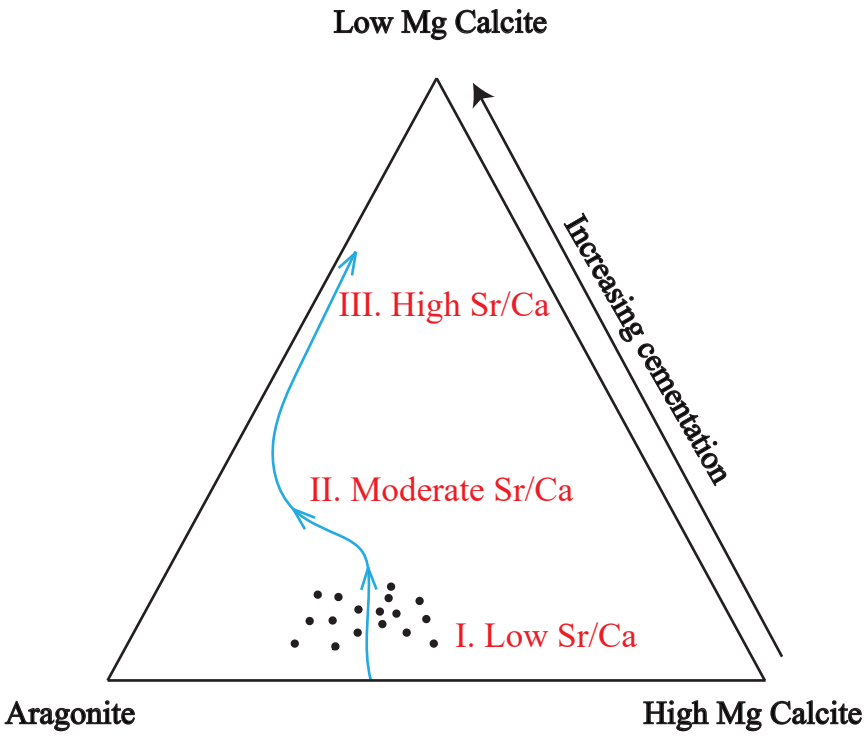

Appendix-C3: Aragonite and high-magnesium calcite are more soluble than low-magnesium calcite in meteoric waters resulting in depleted Mg and Sr levels. I. shows initial cementation, II. shows the loss of Mg then III. the dissolution of aragonites takes place as the cementation process concludes.

Interpretation of element distribution of clusters									
Depth	Sr/Ca	Si/Al	K	Al	Ca	Sr	Zr	Ti	cluster
9484.42	0.03	19.01	0.14	1.07	11.70	0.04	0.03	0.20	1
9484.5	0.03	17.38	0.19	1.18	11.38	0.04	0.03	0.17	1
9484.58	0.03	18.47	0.17	1.13	11.18	0.04	0.06	0.23	1
9484.67	0.04	17.78	0.19	1.20	10.37	0.04	0.03	0.18	1
9484.83	0.04	7.56	0.89	3.08	7.40	0.03	0.03	0.31	3
9484.92	0.04	11.44	0.49	2.01	8.08	0.03	0.04	0.27	3
9485.17	0.03	13.55	0.02	0.94	24.07	0.07	0.01	0.11	2
9485.25	0.03	12.75	0.06	0.86	21.73	0.06	0.01	0.11	2
9485.33	0.03	14.52	0.31	1.60	9.92	0.04	0.03	0.21	2
9485.42	0.03	12.29	0.41	1.88	9.15	0.03	0.06	0.29	3
9485.5	0.03	14.40	0.30	1.65	10.79	0.04	0.03	0.18	2
9485.58	0.03	17.30	0.21	1.34	11.73	0.04	0.03	0.17	1
9485.67	0.03	14.25	0.32	1.60	10.76	0.04	0.04	0.19	2
9486.08	0.03	12.33	0.41	1.82	9.08	0.03	0.03	0.21	3
9486.17	0.03	15.77	0.26	1.41	10.68	0.04	0.03	0.20	2
9486.25	0.04	14.43	0.33	1.56	9.67	0.04	0.03	0.19	3
9486.33	0.03	14.54	0.30	1.58	10.49	0.04	0.03	0.18	2
9486.5	0.03	16.85	0.22	1.43	11.32	0.04	0.03	0.15	2
9486.58	0.03	18.74	0.18	1.17	11.29	0.04	0.03	0.16	1
9486.67	0.03	18.91	0.13	1.07	12.55	0.05	0.06	0.20	1
9486.75	0.03	18.19	0.17	1.17	11.37	0.04	0.05	0.17	1
9486.92	0.05	3.40	2.25	6.26	3.85	0.02	0.03	0.47	3
9487	0.05	5.34	1.34	4.03	4.51	0.03	0.03	0.36	3

The average of each element is calculated:

	Sr/Ca	Si/Al	K	Al	Ca	Sr	Zr	Ti
Average:	0.03	14.31	0.40	1.78	11.00	0.04	0.03	0.21

The average of each element is calculated for each cluster:

	Sr/Ca	Si/Al	K	Al	Ca	Sr	Zr	Ti
1	0.03	18.22	0.17	1.17	11.45	0.04	0.04	0.19
2	0.03	14.58	0.22	1.38	13.72	0.04	0.03	0.17
3	0.04	9.54	0.87	2.95	7.39	0.03	0.04	0.30

Those values are then divided by the overall average of each element:

	Sr/Ca	Si/Al	K	Al	Ca	Sr	Zr	Ti
1	0.98	1.27	0.43	0.65	1.04	1.05	1.20	0.87
2	0.92	1.02	0.55	0.78	1.25	1.13	0.78	0.78
3	1.12	0.67	2.16	1.65	0.67	0.79	1.02	1.40

Average of K(cluster 2)/Average of K= 0.55

Appendix-C4: The average of the elements in each cluster with respect to the overall average weight percent of the elements is used to interpret each cluster. Cluster 1 was interpreted to be the calcareous sandstone as it shows high values of Si/Al, Ca and Sr (1.27, 1.04 and 1.05, respectively). Cluster 3 was interpreted to be a detrital mudstone as it reports high values of Ti, K, Al (1.40, 2.16, 1.65, respectively). This process is used to interpret clusters and to build charts to show the variation of both common and trace element distributions from cluster to cluster

APPENDIX D: Chemofacies classification

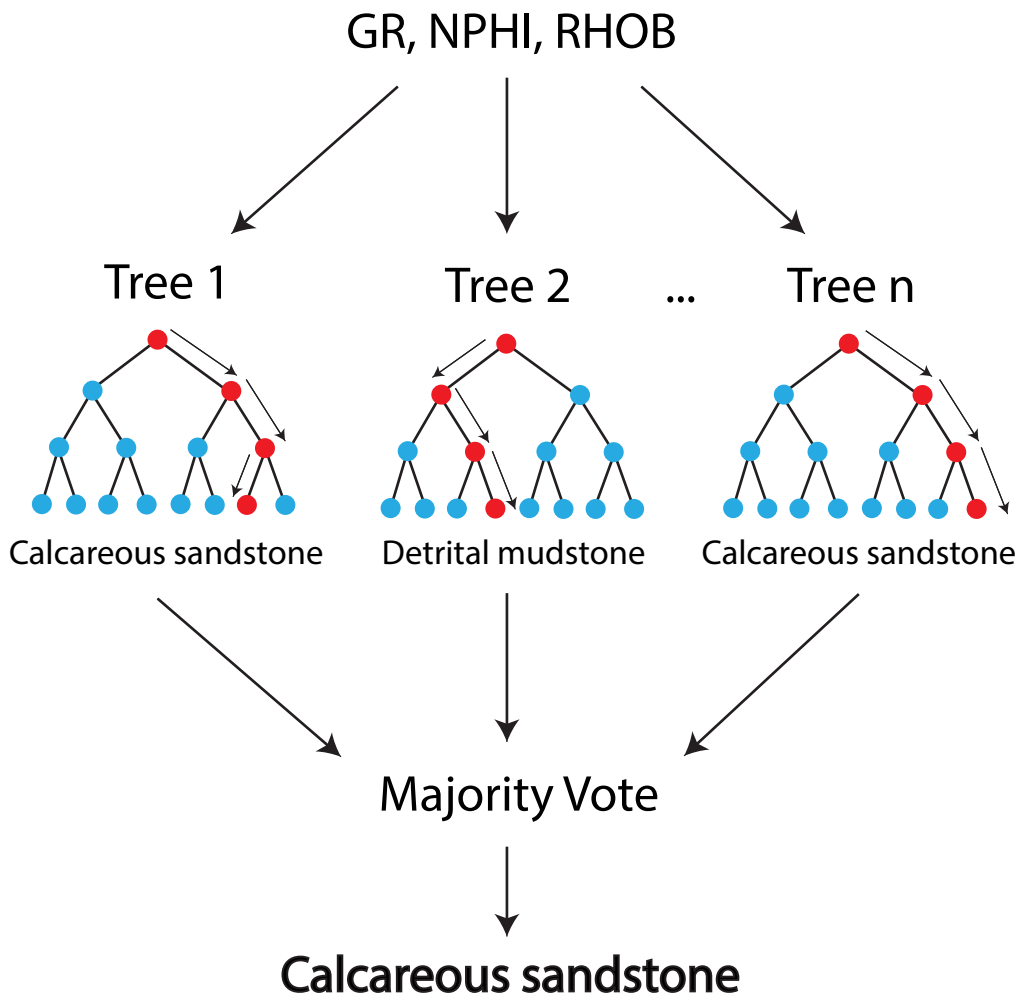

Appendix-D1: Random Forest is a supervised machine learning technique used to classify chemofacies in non-cored wells. Random Forest uses an n amount of decision trees that evaluate the data and produce a prediction based on the input data. The outcomes from all of the decision trees are then put through a majority voting process and a final outcome for that data point is generated. In this research, GR, NPHI and RHOB are the inputs for Random Forest that is used to predict chemofacies.

APPENDIX E: Reservoir Modeling

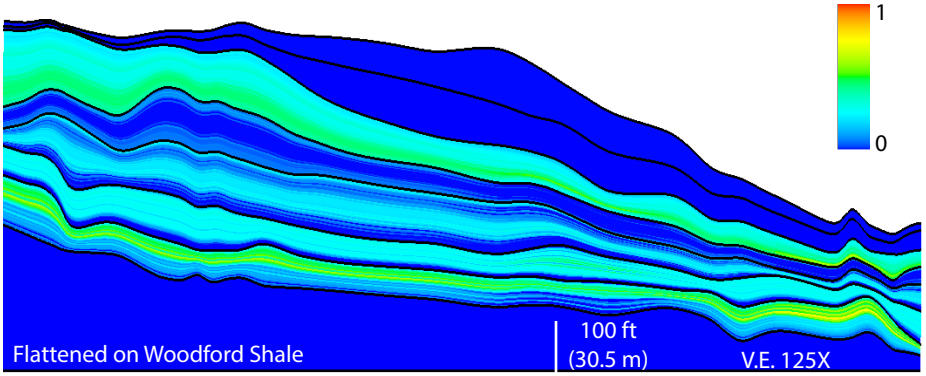

Calcareous sandstone vertical proportion volume

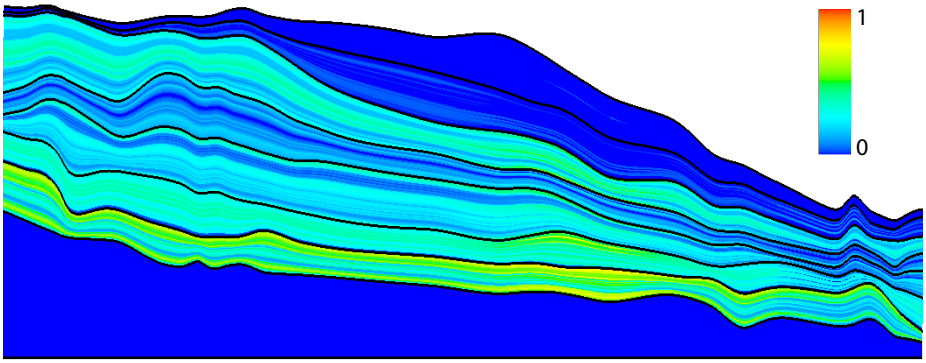

Argillaceous-calcareous siltstone vertical proportion volume

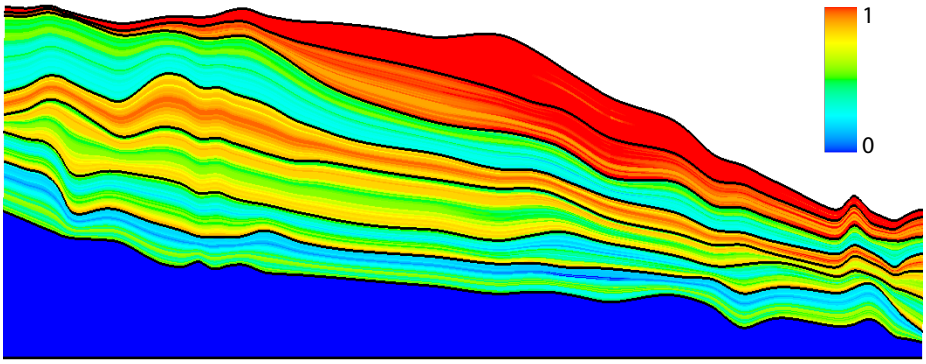

Detrital mudstone vertical proportion volume

Appendix-E1: Vertical proportion volumes are shown for each chemofacies. Chemofacies proportion volumes are created by generating chemofacies vertical proportion curves for each of the 4 geographic zones that were divided for the classification of chemofacies. The vertical proportion curve log data were mapped to generate a proportion volume for each of the 3 chemofacies.

APPENDIX-E2

Variogram Parameters for Chemofacies Modeling (Detrital Mudstone)				
Zone	Major (ft)	Minor (ft)	Vertical (ft)	Azimuth (degrees from N)
Meramec 7	20,000	15,000	4.024	-27
Meramec 6	20,000	15,000	5.395	-27
Meramec 5	20,000	15,000	5.318	-27
Meramec 4	20,000	15,000	2.874	-27
Meramec 3	20,000	15,000	6.701	-27
Meramec 2	20,000	15,000	7.885	-27
Meramec 1	20,000	15,000	5.414	-27
Variogram Parameters for Chemofacies Modeling (Argillaceous-calcareous Siltstone)				
Zone	Major (ft)	Minor (ft)	Vertical (ft)	Azimuth (degrees from N)
Meramec 7	20,000	15,000	3.341	-27
Meramec 6	20,000	15,000	3.189	-27
Meramec 5	20,000	15,000	3.246	-27
Meramec 4	20,000	15,000	2.413	-27
Meramec 3	20,000	15,000	5.981	-27
Meramec 2	20,000	15,000	5.373	-27
Meramec 1	20,000	15,000	5.317	-27
Variogram Parameters for Chemofacies Modeling (Calcareous Sandstone)				
Zone	Major (ft)	Minor (ft)	Vertical (ft)	Azimuth (degrees from N)
Meramec 7	20,000	15,000	1.31	-27
Meramec 6	20,000	15,000	4.592	-27
Meramec 5	20,000	15,000	8.049	-27
Meramec 4	20,000	15,000	5.16	-27
Meramec 3	20,000	15,000	3.12	-27
Meramec 2	20,000	15,000	4.311	-27
Meramec 1	20,000	15,000	4.574	-27

APPENDIX-E3

Variogram Parameters for Rock Type Modeling (Rock Type 1)				
Zone	Major (ft)	Minor (ft)	Vertical (ft)	Azimuth (degrees from N)
Meramec 7	15,000	8,500	4.313	-27
Meramec 6	15,000	8,500	4.095	-27
Meramec 5	15,000	8,500	3.824	-27
Meramec 4	15,000	8,500	2.918	-27
Meramec 3	15,000	8,500	4.151	-27
Meramec 2	15,000	8,500	1.697	-27
Meramec 1	15,000	8,500	2.015	-27
Variogram Parameters for Rock Type Modeling (Rock Type 2)				
Zone	Major (ft)	Minor (ft)	Vertical (ft)	Azimuth (degrees from N)
Meramec 7	15,000	8,500	3.44	-27
Meramec 6	15,000	8,500	3.337	-27
Meramec 5	15,000	8,500	3.241	-27
Meramec 4	15,000	8,500	3.444	-27
Meramec 3	15,000	8,500	3.281	-27
Meramec 2	15,000	8,500	1.955	-27
Meramec 1	15,000	8,500	2.955	-27
Variogram Parameters for Rock Type Modeling (Rock Type 3)				
Zone	Major (ft)	Minor (ft)	Vertical (ft)	Azimuth (degrees from N)
Meramec 7	15,000	8,500	2.227	-27
Meramec 6	15,000	8,500	3.215	-27
Meramec 5	15,000	8,500	3.724	-27
Meramec 4	15,000	8,500	2.108	-27
Meramec 3	15,000	8,500	2.569	-27
Meramec 2	15,000	8,500	2.148	-27
Meramec 1	15,000	8,500	3.491	-27

APPENDIX-E4

Variogram Parameters for Water Saturation Modeling (Detrital mudstone)

Zone	Major (ft)	Minor (ft)	Vertical (ft)	Azimuth (degrees from N)
Meramec 7	10,000	5,000	2.488	-27
Meramec 6	10,000	5,000	3.294	-27
Meramec 5	10,000	5,000	3.947	-27
Meramec 4	10,000	5,000	3.91	-27
Meramec 3	10,000	5,000	3.72	-27
Meramec 2	10,000	5,000	4.002	-27
Meramec 1	10,000	5,000	3.777	-27

Variogram Parameters for Water Saturation Modeling (Argillaceous-calcareous siltstone)

Zone	Major (ft)	Minor (ft)	Vertical (ft)	Azimuth (degrees from N)
Meramec 7	10,000	5,000	3.584	-27
Meramec 6	10,000	5,000	4.635	-27
Meramec 5	10,000	5,000	3.925	-27
Meramec 4	10,000	5,000	3.638	-27
Meramec 3	10,000	5,000	3.821	-27
Meramec 2	10,000	5,000	4.044	-27
Meramec 1	10,000	5,000	3.821	-27

Variogram Parameters for Water Saturation Modeling (Calcareous sandstone)

Zone	Major (ft)	Minor (ft)	Vertical (ft)	Azimuth (degrees from N)
Meramec 7	10,000	5,000	3.589	-27
Meramec 6	10,000	5,000	2.725	-27
Meramec 5	10,000	5,000	3.798	-27
Meramec 4	10,000	5,000	3.944	-27
Meramec 3	10,000	5,000	3.676	-27
Meramec 2	10,000	5,000	2.948	-27
Meramec 1	10,000	5,000	3.806	-27

APPENDIX-E5

Variogram Parameters for Effective Porosity Modeling (Detrital mudstone)

Zone	Major (ft)	Minor (ft)	Vertical (ft)	Azimuth (degrees from N)
Meramec 7	10,000	5,000	2.871	-27
Meramec 6	10,000	5,000	4.41	-27
Meramec 5	10,000	5,000	3.276	-27
Meramec 4	10,000	5,000	4.443	-27
Meramec 3	10,000	5,000	3.587	-27
Meramec 2	10,000	5,000	3.392	-27
Meramec 1	10,000	5,000	3.758	-27

Variogram Parameters for Effective Porosity Modeling (Arg. Cal. siltstone)

Zone	Major (ft)	Minor (ft)	Vertical (ft)	Azimuth (degrees from N)
Meramec 7	10,000	5,000	2.262	-27
Meramec 6	10,000	5,000	2.99	-27
Meramec 5	10,000	5,000	3.416	-27
Meramec 4	10,000	5,000	4.73	-27
Meramec 3	10,000	5,000	3.342	-27
Meramec 2	10,000	5,000	2.855	-27
Meramec 1	10,000	5,000	3.906	-27

Variogram Parameters for Effective Porosity Modeling (Calcareous sandstone)

Zone	Major (ft)	Minor (ft)	Vertical (ft)	Azimuth (degrees from N)
Meramec 7	10,000	5,000	2.912	-27
Meramec 6	10,000	5,000	2.706	-27
Meramec 5	10,000	5,000	3.32	-27
Meramec 4	10,000	5,000	4.116	-27
Meramec 3	10,000	5,000	3.09	-27
Meramec 2	10,000	5,000	3.868	-27
Meramec 1	10,000	5,000	7.582	-27

APPENDIX-E6

Variogram Parameters for Reservoir Quality Modeling (Detrital mudstone)

Zone	Major (ft)	Minor (ft)	Vertical (ft)	Azimuth (degrees from N)
Meramec 7	10,000	5,000	2.878	-27
Meramec 6	10,000	5,000	2.34	-27
Meramec 5	10,000	5,000	3.929	-27
Meramec 4	10,000	5,000	3.891	-27
Meramec 3	10,000	5,000	3.869	-27
Meramec 2	10,000	5,000	3.939	-27
Meramec 1	10,000	5,000	4.029	-27

Variogram Parameters for Resrevoir Quality Modeling (Arg. Cal. siltstone)

Zone	Major (ft)	Minor (ft)	Vertical (ft)	Azimuth (degrees from N)
Meramec 7	10,000	5,000	3.394	-27
Meramec 6	10,000	5,000	3.226	-27
Meramec 5	10,000	5,000	3.777	-27
Meramec 4	10,000	5,000	3.835	-27
Meramec 3	10,000	5,000	3.869	-27
Meramec 2	10,000	5,000	3.873	-27
Meramec 1	10,000	5,000	4.143	-27

Variogram Parameters for Reservoir Quality Modeling (Calcareous sandstone)

Zone	Major (ft)	Minor (ft)	Vertical (ft)	Azimuth (degrees from N)
Meramec 7	10,000	5,000	3.763	-27
Meramec 6	10,000	5,000	1.549	-27
Meramec 5	10,000	5,000	3.94	-27
Meramec 4	10,000	5,000	3.238	-27
Meramec 3	10,000	5,000	3.774	-27
Meramec 2	10,000	5,000	3.298	-27
Meramec 1	10,000	5,000	4.007	-27

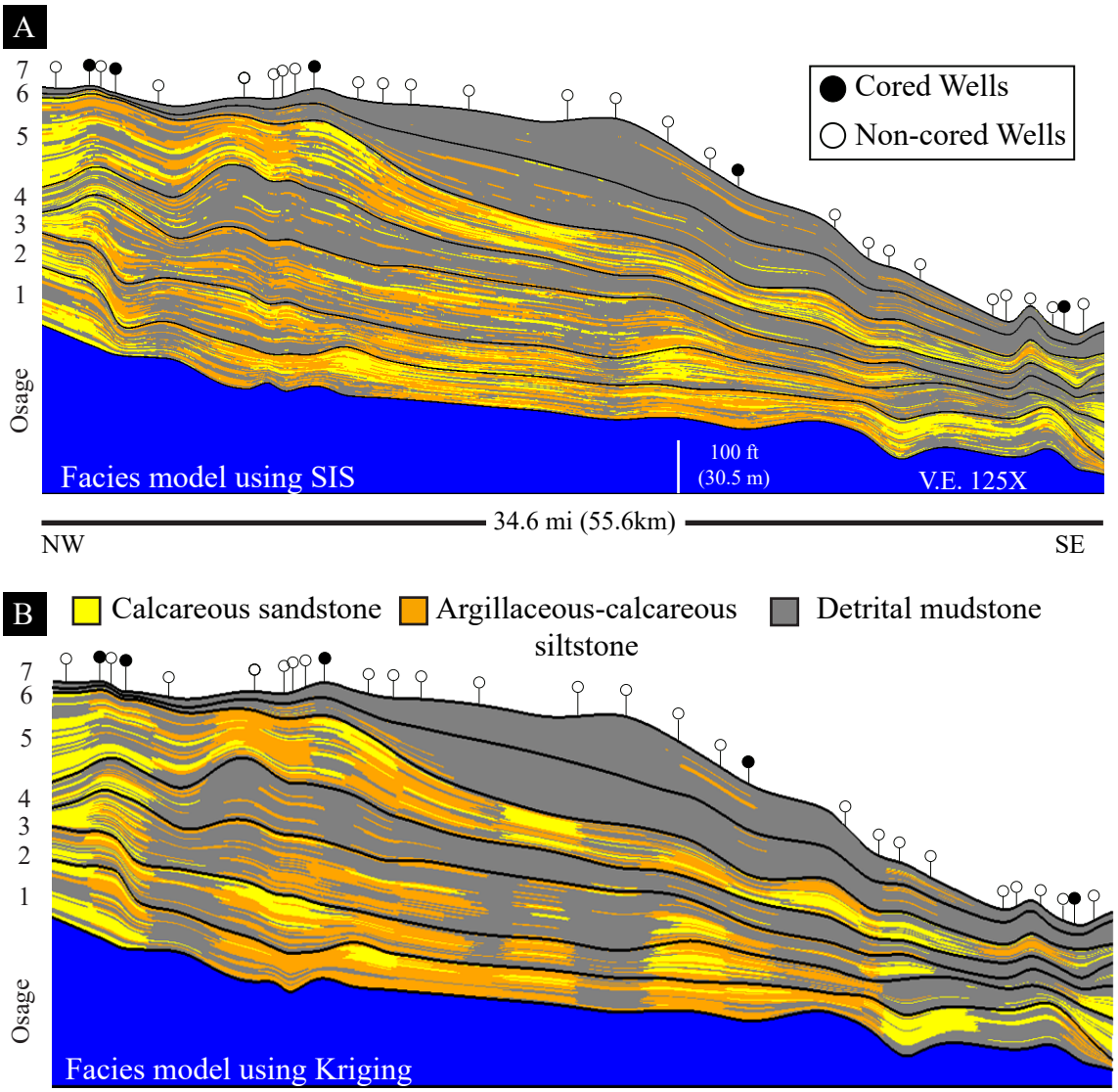

Appendix-E7: The top figure, A, shows the chemofacies model generated using one interation of the sequential-indicator simulation (SIS) modeling method. The figure below, B, was generated using indicator kriging, a method of modeling that results in more averaging and smoothing of chemofacies. Both models were generated using the same horizontal and vertical variogram inputs. The model generated with SIS shows more lateral and vertical heterogeneity whereas the model generated with kriging shows the trends of the chemofacies distribution.

APPENDIX F: Production Analysis

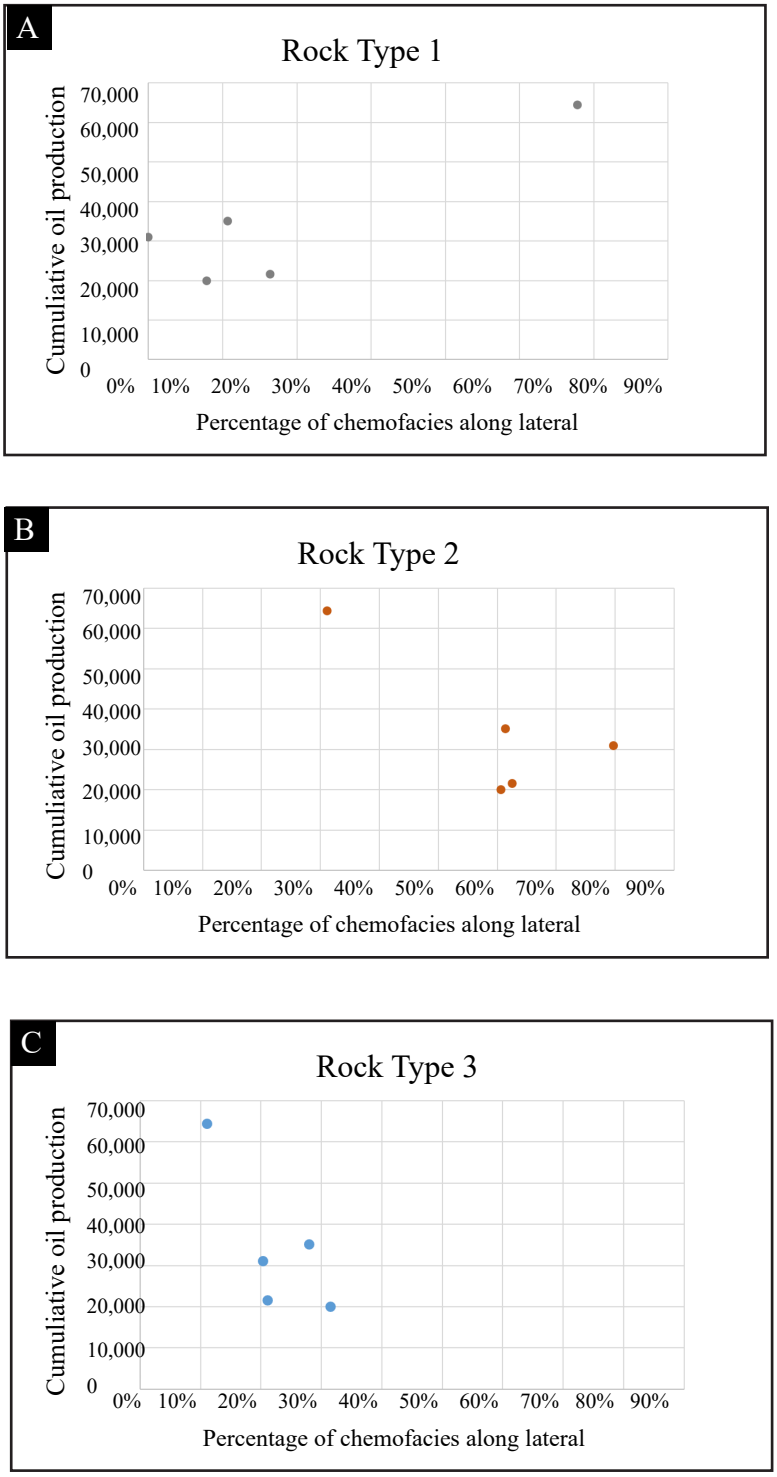

Appendix-F1: Cummulative oil production for 120-days are compared to percenetage of rock types along the lateral for five producing wells. A strong positive correlation between rock type 1 and production is shown, while rock type 2 shows a negative correlation and rock type 3 shows a strong negative correlation with production.